The representation of dry-season low-level clouds over Western Equatorial Africa in reanalyses and historical CMIP6 simulations

P. Camberlin, C F Togbedji, J. Pergaud, A. Berger, R. Aellig, A H Fink, P. Knippertz, V. Moron, N. Philippon

The representation of dry-season low-level clouds over Western Equatorial Africa in reanalyses and historical CMIP6 simulations

P. Camberlin[1], C.F. Togbedji [2], J. Pergaud [1], A. Berger [1], R. Aellig [3], A. H. Fink [3], P. Knippertz [3], V. Moron [4], N. Philippon [5]

(1) Centre de Recherches de Climatologie/Biogéosciences, Université Bourgogne Franche-Comté, Dijon, France - pierre.camberlin@u-bourgogne.fr - Orchid nb : 0000-0003-4896-2332

(2) Université de Paris, Paris, France

(3) Institute of Meteorology and Climate Research, Karlsruhe Institute of Technology, Karlsruhe, Germany

(4) Aix Marseille Univ, CNRS, IRD, INRAE, Coll. de France, CEREGE, Aix en Provence, France & IRI, Columbia University, USA

(5) Institut des Géosciences de l'Environnement (IGE), Univ. Grenoble Alpes, CNRS, IRD, Grenoble INP*, Grenoble, France [*Institute of Engineering and Management Univ. Grenoble Alpes]

Submitted to Climate Dynamics

Declarations

Funding: this work has been carried out as part of the DYVALOCCA project funded in France by ANR (grant ANR-19-CE01-0021) and in Germany by DFG (grant FI-786/5-1)

Conflicts of interest/Competing interests: Not applicable

Availability of data and material: all the data used in this work are publicly available. ISD cloud data are accessible from www.ncdc.noaa.gov/isd/data-access, and EECRA cloud data from NCAR at climateguide.ucar.edu/climate-data. The CALIOP satellite data come from the GCM-Oriented CALIPSO Cloud Product (GOCCP) at climserv.ipsl.polytechnique.fr/cfmip-obs/Calipso_goccp.html. ERA5 reanalyses are available from https://cds.climate.copernicus.eu and MERRA-2 from gmao.gsfc.nasa.gov/reanalysis/MERRA-2/data_access. CMIP6 data can be downloaded from esgf-node.llnl.gov/search/cmip6.

Authors' contributions: Not applicable

Abstract

Western Equatorial Africa (WEA) has a record low sunshine duration during the June–September dry season due to the persistence of low clouds. This study examines the ability of two reanalysis products (ERA5 and MERRA-2) and 8 CMIP6 models (both coupled and atmosphere-only historical simulations) to reproduce the climatology of these low clouds, by comparing it with ground observations and a satellite product. All datasets show a reasonable representation of the regional distribution of low clouds over the Tropical Atlantic and the neighbouring African continent. However, CMIP6 models tend to underestimate the low cloud fraction, especially over WEA in the coupled simulations. This underestimation is partly due to an insufficient seasonal sea-surface temperature (SST) cooling over the Eastern Equatorial Atlantic from April to July in most models, which contributes to reducing the lower-tropospheric stability (LTS). ERA5 data, whose dry season WEA low-cloud fraction is close to observations, indicate that LTS strongly controls the interannual variability of WEA low clouds. Interestingly, the ability to reproduce the mean low cloud fraction does not necessarily scale with the SST biases of the CMIP6 models. The strong dependence of low clouds on interannual SST variations in ERA5 is captured by less than half of the CMIP6 models. Additional key drivers of interannual variations identified in this study, such as Bight of Bonny surface winds and mid-tropospheric temperatures, actually show up inconsistently in CMIP6. Further analyses are needed to disentangle the roles played by SST and independent atmospheric forcings on WEA low cloud formation.

Keywords

cloudiness - sea-surface-temperature - CMIP6 - Equatorial Africa - Equatorial Atlantic Ocean

1. Introduction

Much of climate research focusing on tropical land areas is dedicated to precipitation variability and its driving mechanisms. Dry seasons generally attract less attention, since they are considered as periods of relatively steady, stable and cloudless weather. In Western Equatorial Africa (WEA), especially in Gabon and southern Congo-Brazzaville, the austral winter season from June to September is rainless but is unexpectedly also the time of the year showing the least sunshine and the highest cloud amounts (Bush et al. 2019; Philippon et al. 2021). Over the Mayombe range in Congo-Brazzaville, mean dry season sunshine duration is under one hour per day (Bouka-Biona et al., 1993). The extensive low cloud cover found during this season is associated with relatively low daytime temperatures, which

reduces evapotranspiration and is likely to play a key role in the survival of an evergreen forest in much of the region, despite the long dry season of up to 4 months (Clairac et al. 1989; Couralet et al. 2010 ; Philippon et al. 2019; Réjou-Méchain et al. 2021).

Dry season low-level clouds in WEA tend to be highly persistent, with occurrences above 80% in Gabon based on synoptic observations (Dommo et al., 2018). They usually take the form of a stratocumulus cloud deck with maximum cloud fraction near 850-900 hPa (Dommo et al. 2018). This cloud deck occurs within the southwesterly monsoon flow, which along the coast is about 1000 to 2000 m deep during this season (Lacaux et al. 1992). The monsoon flow is topped by a temperature inversion (Berruex, 1958; Tschirhart, 1959; Trewartha, 1981). While stratocumulus cloud decks are recurrent features over the eastern flanks of subtropical anticyclones covering oceanic areas (Klein and Hartman, 1993; Wood, 2012; Eastman and Warren, 2014), there are more uncommon over equatorial land areas. They are found in Western Africa along the Gulf of Guinea coastal zone (Fink et al. 2011; Knippertz et al. 2011 ; Schrage and Fink, 2012; Schuster et al., 2013 ; Dione et al., 2019; Hannak et al., 2017; Danso et al. 2020), also from July to September, but their frequency is not as high as in Western Equatorial Africa. A stratocumulus cloud cover is also a recurrent feature in austral winter at Nairobi (Kenya), on the east-facing (windward) slopes of the East African Highlands, suggesting a key role of orography (Camberlin, 2018).

Although the WEA low clouds are not strictly a coastal phenomenon, since they extend to about 300-400 km inland (Dommo et al., 2018; Phillipon et al. 2019), their location east of the Equatorial Atlantic Ocean at a time when the seasonal coastal and equatorial upwelling reaches its maximum intensity suggests that sea surface temperature (SST), combined with the onshore low level flow, is an important control. However, the mechanisms of the low cloud formation over this region and its representation in models are not well known. Further south over the Southeast Atlantic Ocean, there is still some uncertainty on the exact role played by the cool marine surface, given the complex feedbacks between clouds and surface temperature (Philander et al. 1996; Trzaska et al. 2007; Bellomo et al. 2015). Adebiyi and Zuidema (2018) found that both meteorological factors (including atmospheric stability and large-scale subsidence) and aerosol forcing (biomass-burning aerosols from Southern Africa) contribute to the development of the persistent low-level cloud deck over this area, while Koseki and Imbol Koungue (2021) showed that March-April low-level clouds were enhanced in years of cold SST anomalies along the Angolan coast (called 'Benguela Niña' events, Shannon et al. 1986). Even further south, for the coastal Namib Desert Andersen et al. (2020) showed that fog and low-cloud occurrence is controlled by variations in cloud-top longwave cooling and the strength of the onshore flow, both modulated by synoptic-scale disturbances.

Uncertainty also revolves around the capability of global circulation models (GCMs) and even reanalysis products to reproduce this low cloud cover. Low clouds are known to be difficult features to model (Dufresne and Bony, 2008; Lauer and Hamilton, 2013; Zelinka et al., 2017; Myers et al. 2021). Over the tropical and subtropical zones, simulated low clouds tend to be too few and too bright, i.e. have an overestimated optical thickness, likely due to a vertical overlap of cloud layers (Nam et al. 2012; Cesana and Walliser, 2016). Within the GCMs participating in the CMIP5 experiment, there is also a large inter-model diversity in the relationship between marine low clouds and SST (Cesana et al. 2019). The poor simulation of marine low clouds should be considered along with the warm SST bias often found over these regions. Hu et al. (2008) suggested that the underestimation of low clouds was by itself a potential cause of the warm SST bias over the southeastern Atlantic Ocean. Xu et al. (2014), however, found that the overestimation of shortwave radiation associated with the insufficient marine low clouds in CMIP5 models was not the leading cause of the warm bias, and hypothesized a role of eddy-induced ocean heat transport. For southern West Africa, Hill et al. (2016) found a strong underestimation of June-July low cloud cover in both ERA-Interim reanalysis data and CMIP5 atmospheric models forced by prescribed SSTs. Hannak et al. (2017), for the same region, analysed a larger number of CMIP5 models and showed that their simulation of low-level clouds was only marginally improved from that of previous generation models (CMIP3). The underestimation of low-cloud cover appears to be related to the subgrid cloud schemes, and to too low near-surface relative humidity at daytime, associated with abundant solar radiation and too high daytime maximum temperatures. No study ever examined the skill of climate models in the simulation of low cloud cover over WEA, despite its temporal persistence during the dry season and major feedbacks on the local climate.

This study will make use of newly available CMIP6 simulations, with the aim to address the following questions: (i) are global climate models and two recent reanalysis products (i.e. ERA5 and MERRA2) capable of realistically representing the low clouds present in WEA? (ii) are the low clouds of this region a mere extension of the large-scale low cloud deck found over the Southeast Atlantic Ocean? (iii) do CMIP6 GCMs underestimate low clouds as in the previous model generations, and is there any difference between atmospheric and coupled simulations? (iv) how does the low cloud cover relate to oceanic and atmospheric forcings, in models and reanalyses? (v) do these relationships help to understand the models' systematic biases in their reproduction of low clouds? To answer these questions, low cloud cover will be compared between CMIP6 historical simulations (both coupled and atmospheric only), both reanalysis products, Cloud-Aerosol Lidar with Orthogonal Polarization (CALIOP) satellite data and in situ synoptic observations for WEA. The focus will be on the austral winter dry period (June–September) during which most of the low clouds develop over the region, but

insights will also be given into the annual cycle. Besides the examination of mean fields, interannual variability will be considered, in particular the relationship between low cloud variability and SST over the Equatorial Atlantic Ocean, which is suspected to play a significant role in (or least interact with) low cloud occurrence.

Section 2 presents the different types of data and the methods used in the study. The climatology of low level clouds is then examined (section 3.1), followed by an analysis of the interannual variations of low clouds (section 3.2). Finally, their relationships with oceanic and atmospheric fields are studied in section 3.3. Section 4 summarizes the results.

2. Data and methods

Four types of data sets are used (Table 1): satellite observations (CALIOP), surface observations (ISD and EECRA), reanalyses (ERA5 and MERRA-2) and simulations from climate models (CMIP6). All the data (with some exceptions as noted below) are extracted over the period 1979–2014, which is common to most data sets, at the monthly timescale. Low cloud definitions vary between these data sets and are presented at the end of this section.

2.1 CALIOP

CALIOP (Cloud-Aerosol Lidar with Orthogonal Polarization) is the lidar device aboard the CALIPSO satellite. CALIPSO (Cloud Aerosol Lidar and Infrared Pathfinder Satellite Observations) is a Franco-American mission launched in 2006 with the objective of studying the radiative impacts of clouds and aerosols on climate. CALIOP is a two-wavelength backscattering lidar (532 and 1064 nm) that provides high-resolution vertical profiles of clouds and aerosols (Chepfer et al., 2008). The lidar detects all types of clouds but low clouds can only be detected when they are not covered by optically thick higher clouds. The data used in this study are not those obtained directly from the lidar but come from the GCM-Oriented CALIPSO Cloud Product (GOCCP) (see below). The spatial resolution of the GOCCP low cloud data is 2° in latitude and 2° in longitude, i.e. approximately a 200 km grid; hence they are used to depict large-scale patterns only. The data are available from June 2006 and extracted up to December 2019.

2.2 ISD

ISD (Integrated Surface Database) is a global database comprising hourly synoptic surface observations made at meteorological stations (Smith et al., 2011). It is a database managed by the United States NCEI (National Centers for Environment Information). It includes over 35,000 stations around the world, with early data dating back to 1901, but many series beginning in the 1970s. Several parameters are recorded in the database such as temperature, wind, cloudiness, precipitation. In Gabon and Congo-Brazzaville, there are 30 stations with cloud data (sky cover, cloud ceiling, types of clouds – low, middle and high) (figure 1a). Only the synoptic hours (i.e. GMT 0000, 0300, 0600 etc.) are retained. Unfortunately, the records are rather incomplete. Only 15 stations have more than 25% of non-missing 3-hourly records over the period of study 1979–2014.

2.3 EECRA

EECRA (Extended Edited Cloud Report Archive) is a global cloud database (Hahn and Warren, 1999). These data are surface observations from various sources which have been processed, edited after quality control, from reports made by observers on ships or on the continent, day and night. Li et al. (2015) found an excellent agreement at global scale between EECRA cloud data and various satellite cloud products. Data from land stations cover the period 1971–2009, from which the sub-period starting in 1979 has been extracted. Low cloud fraction is available at three-hourly resolution. There are only 25 stations in the study area (figure 1b). The overall amount of missing data is close to that of the ISD data set.

2.4 ERA5

ERA5 is the fifth generation of climate reanalysis data from ECMWF (European Centre for Medium-Range Weather Forecasts). ERA5 replaces ERA-Interim, which ceased to be produced at the end of August 2019 (C3S, 2017), and includes considerable improvements and higher horizontal, temporal and vertical resolutions (Hersbach et al. 2020). The data are at a native horizontal resolution of 31 km, made available on a 0.25-degree grid, and resolve the atmosphere at 137 levels from the surface to a height of 80 km, on an hourly time scale. ERA5 uses the Tiedtke cloud scheme (Tiedtke, 1993) to forecast a three-dimensional cloud fraction for each grid box. Monthly data are extracted over the period 1979–2014. In addition to low cloud fraction, the following variables have been used: SST, relative humidity, temperature, zonal and meridional winds at 1000, 925, 850, 700, 600 and 200 hPa. For oceanic and atmospheric fields, the ERA5 reanalyses will serve as the reference.

2.5 MERRA2

MERRA (Modern-Era Retrospective analysis for Research and Applications) produced by NASA (Rienecker et al., 2011) is a second set of reanalyses used in this study. The second generation of these reanalyses (MERRA-2), starting from 1980, is used in this study. It is based on GEOS-5 for the assimilation of the most recent sources of satellite data, in particular new microwave sounders and hyperspectral infrared radiation instruments (Bosilovich et al., 2016). The resolution is 0.625° × 0.5° or approximately a 50km grid. Only low cloud data are extracted from MERRA-2 over the period 1980–2014. The initial time step is 30 minutes, and data are integrated as monthly averages.

2.6 CMIP6

CMIP (Coupled Model Intercomparison Project) is an inter-comparison project of coupled ocean-atmosphere climate models the objective of which is to better understand past, present and future climate change. The project falls under the World Climate Research Program (WCRP) of the World Meteorological Organization (Eyring et al., 2016) and is currently in its sixth phase (CMIP6). Data cover the period 1850–2100 depending on the type of experiment, i.e. natural variability or response to changes in radiative forcing.

The present work seeks to evaluate the models' performance to simulate the recent climate through historical simulations, and projections are therefore not examined. Two types of experiments are selected: coupled simulations and atmosphere-only simulations (AMIP: Atmospheric Model Intercomparison Project). The historical coupled simulations are only forced by observed features such as solar variability, volcanic aerosols, modification of the atmospheric composition (greenhouse gases and aerosols) caused by human activities. These simulations go from 1850 and extend to the near present (2014 in CMIP6). The AMIP-type simulations (hereafter referred to as "atmosphere-only simulations"), on the other hand, can be used to assess the atmospheric response to forcings by surface conditions (especially SSTs) in addition to changes in the composition of the atmosphere. The period of availability of the atmosphere-only simulations is from January 1979 to December 2014.

A total of eight models are used in this study: CNRM (Centre National de Recherches Météorologiques), IPSL (Institut Pierre-Simon-Laplace), E3SM (Energy Exascale Earth System Model), MIROC (Model for Interdisciplinary Research on Climate), MOHC (Met Office Hadley Center), MRI (Meteorological Research Institute), GFDL (Geophysical Fluid Dynamics Laboratory) and NCAR (National Center for Atmospheric Research). The climatic variables are extracted over the period 1979–2014, and comprise low cloud fraction, SST, atmospheric temperature, zonal and meridional wind, and relative humidity.

The number of simulations used per model is provided in table 2. It corresponds to the availability and accessibility of the data at the time of research. In this study all ensemble members available for a given model and experiment are averaged together when analysing mean patterns, but are considered individually when computing correlations.

2.7 Definition of low clouds

Surface synoptic reports from which the ISD and EECRA archives derive are based on human observers' estimates of the cloud fraction of low clouds (LC) as the part of the sky covered by clouds the base height of which is typically below an altitude of 2 km. However, this category includes both stratiform clouds (stratus and stratocumulus) and vertically extensive clouds (cumulus and cumulonimbus). Since the present study is interested in stratiform clouds only, vertically extensive clouds (LC codes 1, 2, 3 and 9) have been excluded from LC observations (i.e., the corresponding cloud fraction is set to zero). We retained LC code 8 (cumulus and stratocumulus with bases at different levels), thus contrary to Schrage and Fink (2012), our LC statistics do not purely refer to stratiform clouds, although this is the overwhelming cloud type for the region and the season. In EECRA, the two extended codes for obscured sky conditions available in this data set (codes 10 and 11, i.e. fog and thunderstorms) have not been considered (low cloud cover similarly set to zero). The cloud fraction initially expressed in octas was converted to percent, and the arithmetic mean was computed to obtain monthly and seasonal averages. In the ISD data set, some records are based on METAR reports, which classify cloud cover in 5 broad categories. For ISD we therefore considered the occurrence of stratiform low clouds by considering the presence of an extensive low cloud cover at the time of observation, defined as an LC fraction greater than or equal to 5 octas (i.e. “broken” or “overcast” in the METAR cloud deck reports). The LC frequency is then simply obtained as the percentage of low cloud observations divided by the total number of synoptic reports at the station. This definition was retained for the ISD dataset only.

Reanalysis products provide LC fraction data but the tropospheric depth over which low clouds are considered differ between ERA5 and MERRA2. In ERA5, low clouds are defined as the integration of all clouds found at pressure levels greater than 0.8 times the local surface pressure, i.e. below about 2 km assuming a standard atmosphere. Importantly, ERA5 LC fraction does not distinguish stratiform from vertically developed clouds, hence it is expected that in seasons when convection is active (outside the JJAS season in the core study area) ERA5 LC fraction is positively biased relative to our station estimate described above. In MERRA2, the LC fraction (“CLDLOW” variable) is described as the maximum of the

total cloud fraction (convective and large scale) of any layer at or below 700 hPa (about 3km in a standard atmosphere).

For CALIOP satellite data, the low cloud definition is the one retained in the GCM-Oriented CALIPSO Cloud Product (GOCCP) (Chepfer et al., 2010). GOCCP was built from an algorithm designed to evaluate the representation of clouds in climate models. Three categories of clouds are differentiated based on pressure level (P): low level (P> 680 hPa), medium level (680 <P <440 hPa) and high level (P <440 hPa). The retrieval steps are described by Chepfer et al. (2013). In this product, low clouds are characterized by the cloud fraction at elevations below 3.2 km (P> 680hPa). The LC fraction is calculated from the CALIPSO simulation included in the second version of the Cloud Feedback Model Intercomparison Project Observational Simulator Package (COSP) (Webb et al., 2017). Although these data can handle multi-layered clouds, the presence of optically thick high clouds and those associated with deep convection within the Intertropical Convergence Zone may partly mask low clouds (Chepfer et al., 2010; Vaughan et al., 2009). For this reason, the difference with the definitions retained in synoptic observations not only lies in the altitude of the top of the lower level, but also to the fact that in one case the clouds are somehow observed "from below" and in the other case "from above".

The data from CALIOP, ISD and EECRA will serve as initial references for the evaluation of CMIP6 and reanalyses. Each of these reference datasets has its own flaws: ISD and EECRA records have lots of gaps and are only available at a limited number of stations, and in CALIOP stratiform low clouds can sometimes be undetectable since they can be hidden by opaque higher clouds of convective origin.

2.8 Methods

Most analyses focus on the JJAS season, which is the dry season in most of WEA and shows the highest frequency of stratiform low clouds (Dommo et al., 2018). JJAS long-term means at individual stations are computed from all available observations (using only stations with at least 300 three-hourly records). Both night- and daytime observations are used, since the CMIP6 data do not enable to investigate the diurnal cycle. Although low clouds are more frequent at night, we checked that both night- and daytime observations were present at the stations we used (i.e., the stations did not close during the whole night), and that the general results of our study were not affected by mixing night- and daytime records. However, observed ISD and EECRA low cloud monthly and seasonal means may be slightly negatively biased because more observations are generally available at daytime (63% of the records are within the time-span 0600-1500 UTC).

The inter-comparison of the data sets is first carried out over a broad area covering an extended Gulf of Guinea area and the neighbouring African land areas (15°W–30°E, 20°S–20°N, figure 2). Then more restricted analyses are produced focusing on WEA, using regional indices which will be defined below. This part of the analysis has some limitations in CMIP6, since the relatively coarse spatial resolution of the simulations (100–250km) do not enable a detailed spatial analysis.

Comparisons between the data sets are made using standard methods. To assess the agreement in the spatial distribution of low clouds, pattern correlation coefficients are computed as well as bias and root-mean-square error (RMSE). To that end, all products are linearly interpolated to the same resolution, i.e. that of ERA5 (about 30 km). The agreement in temporal variations is examined by plotting the mean annual cycle of low clouds and, for the atmosphere-only experiments, reanalyses and observations, by analysing interannual variations using Pearson's correlation coefficient. The latter is also used to relate low clouds and SST variations. In addition, Taylor diagrams are plotted, which enable to compare at the interannual time-scale the skills of different data sets (CMIP6 and MERRA2) with respect to a reference time-series (ERA5), by combining correlations, centered RMSE and standard-deviations.

Two regional low clouds indices are extracted over Gabon, depicting regions where the dry season low cloud cover is the most persistent (figure 1), with coastal and inland locations respectively in order to depict the zonal LC gradient (Dommo et al., 2018). Given the coarse definition of CMIP6 data and the limited availability of synoptic stations, it was not possible to define customized indices reflecting the exact topography, although the latter has some effect on LC patterns. The first index covers north-western Gabon along the coast (9–11°E, 1°S–1.5°N) and the second one is located further inland over north-eastern Gabon (11–13°E, 1.5°S–1.5°N). Each includes three stations from the ISD and EECRA databases, namely Libreville, Cocobeach and Lambaréné (NW-Gabon), and Makokou, Mitzic and Lastoursville (NE-Gabon). Seasonal (JJAS) means for individual years are computed first at station level (based on days with at least 4 three-hourly records, and provided that half the days in a season have data), then the time-series for each station is standardised, and finally a regional average is computed. If in a given year only one station is available, then the average is set to missing.

An SST index is also computed over the region 5–13°E and 2–9°S, i.e. off the coasts of Gabon and Congo-Brazzaville, south of Cape Lopez. This corresponds to the part of the equatorial Atlantic upwelling area ("cold tongue") which shows the largest amplitude (>3.5°C) in the SST annual period (Merle et al., 1980). However, this index is representative of JJAS SST variations over a much larger area covering most of the Eastern Equatorial Atlantic (Servain and Merle, 1993 - not shown).

In order to describe atmospheric stability, a key feature in the development of low clouds (Slingo, 1987; Klein and Hartmann, 1993; Hu et al., 2008; Sun et al. 2011), the Lower-Tropospheric Stability index (LTS) defined by Klein and Hartmann (1993) is used. It is computed over Gabon (10–12°E, 3°S–1°N) as the difference between the potential temperature at 700 and 925 hPa. The 925 hPa pressure level was used instead of 1000 hPa because over land, 1000 hPa temperature is not defined in all the models.

3. Results

3.1 Climatology of low level clouds

The JJAS mean low cloud fraction is first examined over the larger region (Gulf of Guinea and nearby African landmass) (figure 2). CALIOP data shows a major contrast between the oceanic areas, where a high to very high LC fraction is observed (40–85%), especially off the coast of Southern Angola, and the land areas where LC fraction is generally below 20%. As an exception to the land areas, the coastal regions from Sierra Leone to Northern Angola show a higher LC fraction, with a distinct maximum in Gabon (30–70%). This maximum decreases inland, but the LC fraction in the northern Democratic Republic of Congo is still above 20%. The two reanalysis products and the CMIP6 coupled simulations all display high pattern correlations with CALIOP (figure 2, lower right corners). This merely reflects the land-ocean contrast, always well replicated, but it is easy to see that both the oceanic and land patterns often notably differ from the CALIOP satellite estimates. In ERA5 for instance, while the oceanic LC fraction agrees relatively well with satellite data (as found by Koseki and Imbol Koungue, 2021), on the land areas bordering the Gulf of Guinea, the LC fraction is very high, and even over the inland (northern) part of the Congo Basin, it often exceeds 40%. This is likely due to the fact that in ERA5, low clouds include convective clouds with a low cloud base. MIROC also portrays a high LC fraction over the Congo Basin, with almost no difference with the coastal regions. By contrast, an overall negative bias is found in some products, especially MERRA2 reanalysis and CNRM. The IPSL simulations are among the most skilful ones, both in terms of bias and spatial patterns. On the whole however, most CMIP6 simulations tend to underestimate LC fractions over coastal areas north of 10°S and the SE tropical Atlantic.

When using the atmosphere-only simulations instead of the coupled ones (figure 3), most models still underestimate LC fractions. However, there is a substantial increase in oceanic and coastal LC fraction in the IPSL, E3SM, MOHC and CNRM models. There is also a marginal increase in many correlation coefficients, but the geographical patterns are not strongly altered. Only MRI shows a significant

correlation increase (from 0.74 to 0.87), which suggests that in this model the coupling critically affects the simulation of LC.

In order to document LC fraction over Gabon, JJAS averages for the two above-defined regional indices are computed (see figure 1 for their location). Synoptic observations are now added and serve as reference for the other datasets. For NW-Gabon (figure 4a), observed LC frequency (ISD) / LC fraction (EECRA) are both very high (73–74%). CALIOP satellite estimates are somewhat lower (62%), possibly because in some occasions low clouds may be obscured by an upper dense cloud layer. The two reanalyses strongly disagree with ERA5 being very close to observation (70%), while MERRA2 shows unrealistically low LC fraction (22%) in agreement with the large bias seen in figure 3. All the CMIP6 coupled simulations (figure 4, light blue bars) underestimate LC fraction. The range is wide however, with CNRM and E3SM cloud fraction being as low as 26% and MIROC reaching 52%. It is noteworthy that all the atmosphere-only simulations (figure 4, dark blue bars), with the exception of MIROC, yield smaller LC fraction biases. The IPSL model shows a mean over NW-Gabon of 75%, very close to observations, and both MOHC and E3SM have LC fractions near 60%, compared to about 30% in their respective coupled simulations. This suggests that the ocean-atmosphere interactions are important components of LC simulation, and that incorrect feedbacks of clouds or atmospheric dynamics on the state of the upper ocean layers are the potential cause of the LC underestimation over the South Atlantic Ocean and nearby land areas.

For NE-Gabon (figure 4b), quite similar conclusions can be reached. Satellite (CALIOP) and in-situ observations (ISD and EECRA) are very close to each other, with LC fraction / frequency around 60%, i.e. slightly less than in NW-Gabon. ERA5 shows a marginal negative bias, but MERRA2 cloud fraction remains very low (19%). Again, CMIP6 models generally underestimate LC fraction, although atmosphere-only simulations perform a bit better than coupled simulations. The ranking of the models in terms of skill is not the same as for NW-Gabon. For instance, the IPSL model shows a too strong inland decrease of LC fraction. However, the coarse spatial resolution of the models is not fully adequate to depict such gradients, partly controlled by topography, which is oversimplified in global models.

The LC annual cycle in the two regions is plotted in figure 5, for CALIOP, synoptic observations and reanalyses, compared to CMIP6 coupled (panels a-b) and atmosphere-only simulations (panels c-d). Synoptic observations (ISD and EECRA) display a strong annual cycle in NW-Gabon. The JJAS season clearly stands out as the period with the highest LC fraction. Low clouds are less frequent in the wet months, i.e. from October to May. The CALIOP annual cycle agrees well with synoptic observations,

although in the cloudy season, the LC fraction is underestimated, and the peak is shifted to July instead of August in both ISD and EECRA observations. Reanalyses deviate markedly. While for ERA5 the JJAS mean is close to observations, the LC fraction during the rest of the year is too high (45–65% from October to May) compared to synoptic records (20–40%). This is due to the fact that convective clouds with low cloud bases are included in the ERA5 LC fraction. By contrast, the MERRA2 reanalysis shows an underestimation of LC all year round, especially in JJAS as documented above.

CMIP6 coupled simulations (figure 5a) display highly dissimilar patterns. MIROC fails to show any realistic annual cycle, with high values outside the JJAS season. This suggests that, as in ERA5, MIROC's low clouds include deep convective clouds, which are dominant outside the JJAS season. This feature could also explain the high LC fraction over the northern Congo Basin in JJAS in both MIROC and ERA5 (figure 2), since convection is relatively active over this region at this time of the year. MIROC's LC fraction unexpectedly drops in August. However, most of the models are able to reproduce an austral winter LC maximum, but it is systematically too weak, sometimes too early (July in CNRM) or more often, too late (September in MRI and E3SM) compared to synoptic reports. For most models, it is the onset of the cloudy season (i.e. the strong increase in LC fraction in June) which is critical, with low clouds developing too slowly in the models. Wet season LC fractions are much better reproduced by most models, except IPSL, which on the contrary has a dry season maximum closest to observations, though delayed.

Compared to coupled simulations, CMIP6 atmosphere-only simulations (figure 4c) better agree with observations, both in terms of timing and amplitude of the annual cycle. The quick increase of LC fraction between May and June is much better reproduced by the atmospheric models, although still a bit weak, except in MOHC or IPSL. However, the peak of LC is still too early in some models (MOHC, GFDL) or too late in others (E3SM, NCAR, MRI). Notably, MIROC's annual cycle is not improved when compared to the coupled version. On the whole, these results confirm that the atmosphere-ocean coupling is key for the accurate reproduction of LC in the region.

The NE-Gabon annual cycle displays features similar to those of NW-Gabon, except with a smaller amplitude (figure 5b–d). In synoptic observations (ISD and EECRA), both the austral winter maximum is a bit lower (about 65% in July and August) and the wet season cloud fraction a bit higher (30–40%). CALIOP cloud fraction is very close to observations in the cloudy season, but lower (20–30%) in the wet season. Both reanalyses again display too weak annual cycles. Similarly, CMIP6 coupled simulations (figure 5b) do not reproduce well the austral winter LC increase, and their wet season cloudiness is also too low. An improvement is found in the atmosphere-only simulations (figure 5d), which show a

larger amplitude in their annual cycle, but the LC fraction is still too low in most months and most models.

3.2 Interannual variability of low clouds

The interannual variations of the JJAS low clouds in the period 1979-2014 are examined for the two Gabon regional indices, in the observation and in the ERA5 reanalysis. The MERRA2 reanalysis is not used given its strong underestimation of LC fraction during this season. Since CALIOP data are available over a short period of time (2006-2014) only, with few years having simultaneous synoptic records, they are not used here either. The many missing observations in the ISD and EECRA data result in highly discontinuous time-series, especially for NE-Gabon. Nevertheless, ERA5 and observations display variations that are largely in phase (table 2). For NW-Gabon, ERA5 correlates at 0.78 with ISD (significant at $p<0.001$, 26 years) and at 0.77 with EECRA (significant at $p<0.001$, 19 years). For NE-Gabon, ERA5 is also strongly correlated with both EECRA (0.82, significant at $p<0.001$, 18 years) and ISD cloud frequency, although for the latter, the number of years available is small (10 only). These results show that ERA5 performs well at reproducing interannual variations of low clouds over Gabon, despite the fact that this variable is not constrained by assimilated cloud observations and therefore entirely simulated by the ECMWF model. In NW-Gabon (figure 6), most years with an abnormally high LC fraction (e.g. 1982, 1983, 1992, 1994, 2005) and those with a low LC fraction (e.g., 1984, 1988, 1989, 1995, 1996, 1999, 2007) show a reasonable agreement between ERA5 and synoptic observations. The year 1984 is known as a highly singular dry season, with out-of-season heavy convective rains in Gabon, which are consistent with the lower frequency of stratiform low clouds (Buisson, 1984). Interannual variations in NE-Gabon are fairly similar (not shown), though the observed time-series are highly discontinuous. The NE-Index correlates with the NW-index at 0.74 (ISD, 11 years), 0.71 (EECRA, 17 years) and 0.98 (ERA5, 36 years).

In the next step, we examine the ability of the CMIP6 models to reproduce the interannual variations of the LC over the same two regions of Gabon. Solely the atmosphere-only simulations can be analysed since the coupled simulations all have their own internal variability. The ERA5 indices are used as the reference because as demonstrated above, they agree fairly well with observed variations, and they have continuous time-series over the period 1979–2014. The MERRA2 data have been included in the assessment. In NW-Gabon (figure 7a), the CMIP6 models show contrasted skills. Three models, CNRM, IPSL and GFDL, stand out by their high correlations with ERA5 (0.64 to 0.72, all significant at $p<0.001$), with a similar and relatively low RMSE (around 3.9%). However, while IPSL and GFDL standard-deviations match that of ERA5, it is too low in CNRM. A lower correlation is found for NCAR (0.45),

while all other models (MRI, E3SM, MOHC) show insignificant or even negative correlations with ERA5. The MERRA2 reanalysis is characterised by a very small standard-deviation, reflecting the large negative bias as discussed above, and its correlation with ERA5 is only modest (0.45).

Overall, the same observations and ranking of models can be made for the NE-Gabon index (not shown). However, correlations with ERA5 are generally lower than in NW-Gabon, and the RMSE is generally higher. Again, GFDL stands out as the model with the best skill.

3.3 Relationships with sea-surface temperature

The inferior performance of the coupled simulations compared to atmosphere-only simulations point to a key role of oceanic dynamics in the adequate simulation of low clouds. Dommo et al. (2018) also suggest that the seasonal occurrence of cool SST off Gabon is instrumental in low cloud genesis. This section thus analyses SST patterns and variability over the South Atlantic Ocean. In Figure 8, the JJAS mean SST is mapped for the eight CMIP6 coupled models (panels b to i) and for the ERA5 reanalysis as a reference (panel a). ERA5 distinctly shows a northward SST gradient, with cold water (<20°C) along the coast of Namibia and southern Angola (ca. 15–20°S), associated with the Benguela Current and coastal upwelling, and warm water north of the equator (>26°C). A zonal band of relatively cool water (23–25°C) is found slightly south of the equator, denoting the Equatorial Atlantic upwelling zone (cold tongue area). The temperature does not exceed 23°C along the coasts from northern Angola to Cape Lopez in Gabon. In all the CMIP6 models, SSTs are biased high in the southeast Atlantic Ocean, including along the coasts of Congo-Brazzaville and Gabon. Likewise, the equatorial cold tongue is missing in most models, or it is too weak and does not extend far enough to the east, like in MIROC or GFDL. Of all the CMIP6 models, MRI and to some extent IPSL seem to best reproduce SSTs over the Atlantic and along the Gulf of Guinea coasts during JJAS, although temperatures are overestimated by about 2°C on average. In MRI the equatorial upwelling extends well towards the coasts of Gabon and Congo-Brazzaville, where the ocean temperature drops to 23°C as in ERA5.

In order to better describe the SST along the Gabonese coast, a regional index is extracted for the area boxed in blue on figure 8a. The annual cycle is plotted in figure 9 to find out whether the poor replication of the JJAS SST in CMIP6 is a result of a flawed seasonal cooling. All the models overestimate SST off the southern coast of Gabon except for – to some extent – MRI. The austral winter cooling is reproduced by all models, but it is noteworthy that it starts too late and is too weak. While in ERA5 the warmest water is found in March (29°C), with a strong cooling starting after April, in most models the SST drops too late and too slowly. Simulated minimum temperature is generally found in August, a bit

late compared to ERA5, and is not cold enough (positive bias of 3–4°C). The models that are best able to reproduce the equatorial upwelling (IPSL and especially MRI) are the only ones to show a quick SST drop from May to July which almost matches that of ERA5, although the minimum austral winter temperature is still overestimated.

Figure 10 shows the correlation between interannual variations of LC fraction (JJAS average) in NW-Gabon and SST at each grid point, within each data set (e.g., ERA5 cloud fraction with ERA5 SST, CNRM cloud fraction with CNRM SST etc.). For ERA5 (figure 10a), the correlation is generally negative over the Equatorial Atlantic Ocean, which indicates that the years showing a high LC fraction in Gabon coincide with cooler ocean temperature than usual. Reciprocally, anomalously warm years such as 1984, 1988, 1995, 1998, 1999, 2003 and 2007 generally coincide with less low clouds in Gabon (figure 6). The correlation coefficients exceed 0.75 (significant at $p<0.001$) in the Eastern Equatorial basin. The correlation maps for LC fraction in NE-Gabon display similar patterns to those of NW-Gabon except that the correlations are generally slightly lower. The use of the SST index extracted off the coasts of southern Gabon and Congo-Brazzaville confirms the very strong negative correlation with ERA5 LC fraction in the two regions (NW-Gabon: -0.81, NE-Gabon: -0.76).

CMIP6 coupled simulations (figures 10b-i) display correlation patterns with NW-Gabon LC fraction that differ largely between models. Two of the eight models, MIROC and NCAR, show non-significant correlations (either slightly positive or slightly negative). The others have negative and significant correlations ($p<0.05$) in agreement with ERA5, but the patterns and intensity are sometimes quite different from those observed. In most of them (IPSL, E3SM, MOHC, GFDL), the highest negative correlations are generally found in the equatorial upwelling area south of the equator. They more or less expand eastward and southward to the African coast from Gabon to Namibia. This pattern is relatively close to that observed from ERA5 data. For NW-Gabon, E3SM and GFDL (figures 10d & 10h) clearly show the strongest negative correlations (< -0.75), which best agree with ERA5, though some inaccurate positive correlations are found along the West African coast and in the southwestern Atlantic. The GFDL negative correlations tend to get a bit weaker for NE-Gabon (not shown). MRI exhibits correlations which are quite uniform but weak, and CNRM displays an unrealistic pattern.

Over the period 1979–2014, there is a significant warming trend over the South Atlantic Ocean in all the eight coupled models but GFDL (not shown). When the linear trend is removed, the correlations are generally slightly enhanced for the models which were already showing an SST-low clouds relationship. Although difficult to transpose to climate change issues, this suggests that a warming trend may not necessarily result in less low clouds over Gabon.

Figure 11 shows the scatter-plots of NW-Gabon LC fraction vs. SST off southern Gabon, where each dot is the JJAS average of a given year, with colours and symbols referring to each of the 8 coupled models (with black stars showing ERA5). An important feature is that the LC bias does not necessarily scale with the SST bias. In other words, the models that most strongly underestimate LC are not necessarily the ones showing the highest SST. For instance, compared to MIROC, MRI only weakly overestimates SST, but has a larger low cloud bias than MIROC. In terms of interannual correlations between LC and SST, the models perform inconsistently. Regression lines are plotted only for the models that show a statistically significant linear relationship between interannual variations of LC and SST. Three models (E3SM, GFDL and IPSL) display very strong negative correlations, as for ERA5. The others either underestimate the relationship or completely miss it. Models that exhibit unsuitably low interannual SST variations tend to miss the relationship with the LC fraction (e.g., CNRM, MIROC, NCAR). GFDL and E3SM, which have the strongest negative correlation with SST (-0.78 and -0.93, respectively) also displays the largest interannual variability, with SSTs varying between 25 and 28.5°C, a range similar to that of ERA5, although (like in other models) SSTs are much too high. However, the correlation between low cloud and SST is unrelated to biases: while MRI has smaller biases compared to E3SM, its correlation is much lower than E3SM.

In order to further understand the origin of the poor performance of several models, the same correlation maps as in figure 10 are produced using the atmosphere-only simulations instead of the coupled ones (figure 12). Almost all the models now reproduce a negative correlation between LC fraction and SST in the Equatorial Atlantic. Compared to ERA5, the spatial pattern and amplitude of the correlation are very accurate in the CNRM, IPSL, MOHC, E3SM and GFDL models. Correlations are a bit too weak in NCAR and MRI, while MIROC portrays a positive correlation, confirming that low clouds captured over Gabon in this model are mainly convective clouds. These results show that much of the flaws in the relationship between SST and cloud fraction in the coupled simulations arise from faulty ocean-atmosphere feedbacks.

3.4 Relationships with atmospheric fields

In order to determine whether the SST-cloud relationship involves variations in atmospheric stability, a lower-tropospheric stability index (LTS) is extracted over Gabon. The scatter-plot of NW-Gabon LC fraction versus LTS shows a very strong interannual correlation (r=0.91) in ERA5 (figure 13). As expected, increased stability is key to the development of a stratiform low cloud cover. This relationship is reproduced by a majority of models. Three of them (IPSL, E3SM and NCAR) show correlations similar to ERA5. Three others have much weaker but significant ($p<0.05$) correlations: MIROC, MOHC and MRI. No relationship is found for CNRM and GFDL. Interestingly, although stability

is supposed to be largely constrained by SST, the models which skilfully reproduce the relationship between LC fraction and stability are not always the same as those which are good at simulating the relationship with SST. E3SM and IPSL reproduce both relationships. By contrast, NCAR and MIROC show a good fit between low clouds and stability, but not with SST. This suggests that in these models climatic forcings other SST (possible mid-tropospheric air temperature) have a dominant control on stability. Conversely, low clouds variability in GFDL is related to SST, but it fails to show any clear relationship with LTS. Overall, these results indicate that the poor simulation of low clouds in the CMIP6 models may be due to a variety of reasons. While the incorrect simulation of SST and association with low clouds is a key feature, purely atmospheric issues are also at play in many models.

While the detailed assessment of these failures is beyond the scope of this paper, figure 14 highlights some atmospheric variables which show a significant relationship with LC fraction over NW-Gabon in ERA5 (top panels). Near-surface winds display positive correlations in the Gulf of Guinea area north of the equator, particularly the Bight of Bonny (both U and V), indicative of an enhanced southwesterly monsoon flow in years with an increased cloud fraction. A stronger monsoon flow north of the equator was found to result from an SST drop in the cold tongue area around the start of the first Guinean rainy season (Leduc-Leballeur et al. 2013; Meynadier at al. 2016). Therefore, the positive correlations between LC fraction and U1000 and V1000 reflect the role of SST on both winds and cloudiness. However, at 850 hPa the correlations with the meridional wind flow turn negative (figure 14), suggesting that the monsoon depth is reduced when the LC fraction is high. This pattern, together with the stronger near surface meridional winds, is indicative of stronger but shallower monsoon flow. This combination is only possible in an environment of higher vertical stability, where turbulent mixing is suppressed and where moisture is concentrated in a shallower layer to allow a more persistent stratiform cloud cover. Potentially, increased surface fluxes due to the higher wind speeds further support this process.

At 700 hPa (above the monsoon flow), a weak positive correlation between LC and temperature is found over Gabon and neighbouring regions (figure 14, top right panel). Together with the negative correlation with surface temperature and SST, this is in line with the strong relationship found above between LTS and low clouds, since a warmer mid-troposphere (colder lower-troposphere) increases low-level stability.

By extracting regionally-averaged indices representative of these relationships (yellow boxes on top panels of figure 14), it is found that the models unevenly reproduce the relationships found in ERA5 (central panels). In particular, the connection with meridional wind is often poorly represented. E3SM

and NCAR perform best in this respect. Only E3SM, MOHC and MRI consistently reproduce the relationships with U1000, V1000 and V850.

In order to find out whether these atmospheric dynamics are related to SST variations, partial correlations are computed between low clouds and the same atmospheric indices, after removing the effect of Eastern Equatorial Atlantic SST (figure 14, bottom panels). In ERA5, the correlation with meridional winds (V1000) becomes very low, indicating that the above wind signal was strongly associated with SST-induced north-south temperature gradients. The correlation with V1000 becomes generally weaker in the models as well, though still significant in E3SM, MRI and NCAR, which for the latter two is no surprise given their poor skills at reproducing SST variations. Note that the near-surface zonal wind flow, by contrast, remains in many models significantly correlated to low clouds after removing the effect of SST, suggesting that other features (possibly land surface warming) also drive the strength of the westerlies. The fact that these partial correlations remain significant while they are not any more in ERA5 is also due to the generally underestimated relationship with SST in several models. The same remarks apply to V850.

Partial correlations with 700 hPa temperature (figure 14, bottom-right panel) are significant, and even stronger than the total correlations, in both ERA5 and several models. This shows that mid-tropospheric warming has a distinct effect on the occurrence of low clouds. It is conceivable that this variable is influenced by processes such as advection or longwave cooling associated with variations in free-tropospheric water vapour or high-level clouds (see e.g. discussions in Andersen et al., 2020).

4. Conclusions

Stratiform low clouds are a recurrent feature of the Southeast Atlantic Ocean. In austral winter, they extend over southern West Africa and Western Equatorial Africa, and mean cloud fractions of more than 60–70% are found over Gabon and southern Congo-Brazzaville. This extensive low cloud cover during the dry season is suspected to play a key role in the presence of a rainforest over WEA, by reducing solar radiation, daytime temperatures and hence water demand. The present paper aimed at assessing the ability of reanalysis products (MERRA2 and ERA5) and CMIP6 models to simulate these low clouds and their drivers, by focusing on mean patterns and interannual variability. CALIOP satellite data and ground observations at synoptic stations were used as reference.

Over the broader region (Equatorial Atlantic and Tropical Africa), the spatial patterns of mean low cloud occurrence as depicted by CALIOP data are reasonably well reproduced by CMIP6 models, ERA5 and MERRA2 reanalyses. However, the mean cloud fraction is severely underestimated in MERRA-2

and in several models, as earlier shown for CNRM for instance (Voldoire et al. 2019). In WEA in particular, most data sets struggle to correctly reproduce the amplitude of the annual cycle and underestimate the JJAS low cloud fraction, with respect to synoptic reports at stations in Gabon. Although MERRA-2 reanalysis shows very good skill in reproducing precipitation and winds in Central Equatorial Africa (Hua et al. 2019), it severely underestimates low clouds. An underestimation of the total cloud fraction in MERRA2 was found for China by Feng and Wang (2019), leading to an overestimation of solar radiation. By contrast, ERA5 reanalysis is fairly accurate in simulating low clouds in WEA during the austral winter, but produces too many low clouds in the rest of the year, probably due to the fact that convective clouds are not discriminated from stratiform clouds in ERA5 as done in this paper for the reference station observations.

Interestingly, the underestimation of low clouds is generally reduced in atmospheric models forced by observed SST compared to coupled ocean-atmosphere models. This suggests that part of the inaccuracies in low cloud simulations is related to unrealistic simulated SSTs. The seasonal development of low clouds in WEA is primarily associated with the surface cooling of the Equatorial Atlantic Ocean between April and July. This cooling is delayed and too weak (2–4°C in most models, instead of 5–6°C) in the CMIP6 coupled models. Richter and Tokinaga (2020) also noted the warm bias in the Equatorial Atlantic in CMIP6, with little improvement upon CMIP5 simulations, and attributed it to the response to wind forcing being too weak. This warm bias reduces the stability of the lower troposphere, which may account for the underestimation of stratiform low clouds. This is in agreement with the observations by Cesana et al. (2012) on the links between SST and low clouds. However, we note that over WEA, the inter-model variations in the low cloud biases do not necessarily scale with their respective SST biases, suggesting that additional factors are at play.

At the interannual timescale, ERA5 variations of low cloud cover match reasonably well those of observed data. These variations are inconsistently reproduced by the atmosphere-only simulations forced by observed SSTs. The GFDL, IPSL and CNRM AMIP-type models show the best correlations ($r \sim 0.65–0.70$ for NW-Gabon over the period 1979–2014). ERA5 data reveal that these interannual variations in low cloud cover are strongly related to SST over a large part of the Equatorial Atlantic Ocean, with correlations exceeding 0.7 in the equatorial upwelling area and off the coasts of Gabon and Congo-Brazzaville. Some models underestimate this relationship, and others completely miss it. The accuracy of the correlation between SST and low cloud variations is only loosely related to the mean biases of the models. Several models display a mean JJAS SST off Gabon exceeding 26°C, an often used threshold for deep convection (Zhang, 1993), whereas in the observation SST over the same region is close to 23.5°C. Yet some of these models, especially E3SM, adequately simulate a strong

relationship between low clouds and SST. However, models whose SSTs are always above 26°C fail to show any strong relationship with low clouds (yet some of them display fairly high and variable LC fraction), suggesting that above this threshold low cloud formation obeys to other forcings in these models.

A preliminary analysis of atmospheric patterns associated with interannual low cloud variations has been carried out in order to suggest possible explanations for the poor low cloud simulations, in addition to the SST biases. Interannual variations of lower-tropospheric stability (LTS) are strongly correlated to low cloud fraction (r=0.91 over Gabon in ERA5). Mean LTS is markedly underestimated in all coupled CMIP6 models, mainly as a result of too high SSTs. While the relationship of LTS with low clouds is correctly simulated by half of the models, others display correlations much lower than in ERA5 or even fail to show any relationship. In some cases (e.g., CNRM, MIROC), this reflects the poorly simulated SST-low cloud relationship. In GFDL however, while the SST forcing on low clouds is well reproduced, the relationship with LTS is not, suggesting that in this case the mid-tropospheric temperature fields are faulty.

ERA5 correlations actually show that low cloud cover over WEA is not only controlled by SST. Surface zonal winds and 700 hPa temperature, partly independent of SST, exert secondary controls on interannual variations of low cloud occurrence. Only about half of the CMIP6 models reproduce these controls. Reanalysis data analysed by Neupane (2016) indicate that the strength of zonal circulation over WEA is controlled by west-east temperature gradients, hence by Congo Basin temperatures in addition to Equatorial Atlantic SST. Among other parameters, biomass-burning aerosols are suspected to play a role in low cloud fraction over the South-East Atlantic Ocean, likely through an additional radiative heating generated by smoke above the low-level clouds, which increases the stability of the low-level inversion, a feedback which is not well represented in many CMIP6 models (Lu et al., 2018; Mallet et al., 2021). However, over WEA, this effect seems moderate only (3-5 % increase of simulated low cloud fraction over southern Congo-Brazzaville when aerosols are activated in the models, according to Mallet et al. 2020).

On the whole, the above results show that the models' imperfect simulation of WEA low clouds has different origins, though realistic SSTs are a key component. Even if biases in mean patterns are not always deterrent to a fair simulation of interannual variations and associated forcing mechanisms, an improved simulation of the coupled ocean-atmosphere dynamics in the region would be key for reliably assessing future low cloud trends over WEA as a result of global warming. Further work also

needs to be carried out on the within-season changes in low cloud occurrence and their forcing mechanisms.

Acknowledgements

This study is part of the project DYVALOCCA (https://dyvalocca.osug.fr/) funded by ANR and DFG under contracts ANR-19-CE01-0021 and DFG FI 786/5-1. Computations were performed using HPC resources from DNUM CCUB (Centre de Calcul de l'Université de Bourgogne), Dijon, France.

674 References

675 Adebiyi AA, Zuidema P (2018) Low cloud cover sensitivity to biomass-burning aerosols and
676 meteorology over the southeast Atlantic. J. Climate, 31(11), 4329-4346. https://doi.org/10.1175/JCLI-
677 D-17-0406.1

678 Andersen H, Cermak J, Fuchs J, Knippertz P, Gaetani M, Quinting J, ... & Vogt R (2020) Synoptic-scale
679 controls of fog and low-cloud variability in the Namib Desert. Atmospheric Chemistry and Physics,
680 20(6), 3415-3438.

681 Bellomo K, Clement AC, Mauritsen T, Rädel G, Stevens B (2015) The influence of cloud feedbacks on
682 equatorial Atlantic variability. J Climate, 28(7), 2725-2744.

683 Berruex M (1958) Contribution à la connaissance de l'atmosphère équatoriale: une année de
684 radiosondages à Léopoldville. Acad. Roy. Sc. Col. Mém., 5(5): 79 p.

685 Bosilovich MG, Lucchesi R, Suarez M (2016) MERRA-2: File Specification. GMAO Office Note No.9
686 (Version 1.1), 73p. Retrieved from http://gmao.gsfc.nasa.gov/pubs/office_notes.

687 Bouka-Biona C, Benech B, Druillet A, Minga A, Nganga D (1993) Evolution thermodynamique diurne
688 de l'atmosphère dans et au-dessus de la forêt du Mayombe en saison sèche, in Echange foret
689 atmosphère en milieu tropical humide, Cros et al., Eds. Unesco, Paris, 11-38.

690 Bush ER, Jeffery K, Bunnefeld N, Tutin C, Musgrave R, Moussavou G, Makaga L (2019) Ground data
691 confirm warming and drying are at a critical level for forest survival in western equatorial Africa (No.
692 e27848v1). PeerJ Preprints doi:10.7287/peerj.preprints.27848v1

693 Camberlin P (2018) Climate of Eastern Africa. Oxford Research Encyclopedia of Climate Science.
694 Retrieved from
695 http://climatescience.oxfordre.com/view/10.1093/acrefore/9780190228620.001.0001/acrefore-
696 9780190228620-e-512

697 Cesana G, Kay JE, Chepfer H, English JM, De Boer G (2012) Ubiquitous low-level liquid-containing
698 Arctic clouds: New observations and climate model constraints from CALIPSO-GOCCP. Geophys Res
699 Lett, 39(20). https://doi.org/10.1029/2012GL053385

700 Cesana G, Waliser DE (2016) Characterizing and understanding systematic biases in the vertical
701 structure of clouds in CMIP5/CFMIP2 models, Geophys Res Lett,43, doi:10.1002/2016GL070515.

702 Cheng A, Xu KM (2015) Improved Low-Cloud Simulation from the Community Atmosphere Model
703 with an Advanced Third-Order Turbulence Closure. J Climate, 28(14), 5737–5762.
704 https://doi.org/10.1175/JCLI-D-14-00776.1

705 Chepfer H, Bony S, Winker D, Cesana G, Dufresne JL, Minnis P, Zeng S (2010) The GCM-oriented
706 CALIPSO cloud product (CALIPSO-GOCCP). J Geophys Res Atmospheres, 115(5).
707 https://doi.org/10.1029/2009JD012251

708 Chepfer H, Bony S, Winker D, Chiriaco M, Dufresne JL, Sèze G (2008) Use of CALIPSO lidar
709 observations to evaluate the cloudiness simulated by a climate model. Geophys Res Lett, 35(15),
710 L15704. https://doi.org/10.1029/2008GL034207

711 Chepfer H, Cesana G, Winker D, Getzewich B, Vaughan M, Liu Z (2013) Comparison of Two Different
712 Cloud Climatologies Derived from CALIOP-Attenuated Backscattered Measurements (Level 1): The

713 CALIPSO -ST and the CALIPSO -GOCCP. J Atmospheric and Oceanic Technology, 30(4), 725–744.
714 https://doi.org/10.1175/JTECH-D-12-00057.1

715 Clairac B, Cros B, Senechal J (1989) Le climat du Mayombe. In: Revue des connaissances sur le
716 Mayombe. PNUD, MAB, UNESCO, Paris, pp 47–68.

717 Copernicus Climate Change Service (C3S) (2017) ERA5: Fifth generation of ECMWF atmospheric
718 reanalyses of the global climate. Retrieved March 5, 2020, from Copernicus Climate Change Service
719 Climate Data Store (CDS). https://cds.climate.copernicus.eu/cdsapp#!/home

720 Couralet C, Sterck FJ, Sass-Klaassen U, Van Acker J, Beeckman H (2010) Species-specific growth
721 responses to climate variations in understory trees of a Central African rain forest. Biotropica, 42(4),
722 503-511.

723 Danso DK, Anquetin S, Diedhiou A, Kouadio K, Kobea AT (2020) Daytime low-level clouds in West
724 Africa–occurrence, associated drivers, and shortwave radiation attenuation. Earth System Dynamics,
725 11(4), 1133-1152. https://doi.org/10.5194/esd-11-1133-2020

726 Dione C, Lohou F, Lothon M, Adler B, Babić K, Kalthoff N, … Gabella O (2019) Low-level stratiform
727 clouds and dynamical features observed within the southern West African monsoon. Atmospheric
728 Chemistry and Physics, 19(13), 8979–8997. https://doi.org/10.5194/acp-19-8979-2019

729 Dommo A, Philippon N, Vondou DA, Sèze G, Eastman R (2018) The June–September Low Cloud Cover
730 in Western Central Africa: Mean Spatial Distribution and Diurnal Evolution, and Associated
731 Atmospheric Dynamics. J Climate, 31(23), 9585–9603. https://doi.org/10.1175/JCLI-D-17-0082.1

732 Eastman R, Warren SG (2014). Diurnal Cycles of Cumulus, Cumulonimbus, Stratus, Stratocumulus,
733 and Fog from Surface Observations over Land and Ocean. J Climate, 27(6), 2386–2404.
734 https://doi.org/10.1175/JCLI-D-13-00352.1

735 Eyring V, Bony S, Meehl GA, Senior CA, Stevens B, Stouffer RJ, Taylor KE (2016) Overview of the
736 Coupled Model Intercomparison Project Phase 6 (CMIP6) experimental design and organization.
737 Geoscientific Model Development, 9(5), 1937–1958. https://doi.org/10.5194/gmd-9-1937-2016

738 Feng F, Wang K (2019) Does the modern-era retrospective analysis for research and applications-2
739 aerosol reanalysis introduce an improvement in the simulation of surface solar radiation over China?
740 Int J Climatology, 39(3), 1305–1318. https://doi.org/10.1002/joc.5881

741 Fink AH, Schuster R, Trentmann J, Schrage JM, Yorke C (2011) Ultra-low clouds over the southern
742 West African monsoon region. Geophys. Res. Lett., 38, L21808,
743 https://doi.org/10.1029/2011GL049278

744 Hahn CJ, Warren SG (1999) Extended Edited Synoptic Cloud Reports from Ships and Land Stations
745 Over the Globe, 1952-1996. Oak Ridge, TN: Carbon Dioxide Information Analysis Center,
746 https://doi.org/10.2172/12532

747 Hannak L, Knippertz P, Fink AH, Kniffka A, Pante G (2017) Why Do Global Climate Models Struggle to
748 Represent Low-Level Clouds in the West African Summer Monsoon? J Climate, 30(5), 1665–1687.
749 https://doi.org/10.1175/JCLI-D-16-0451.1

750 Hersbach H, and Coauthors (2020) The ERA5 global reanalysis. Quart J Roy Meteor Soc, 146, 714,
751 1999–2049, doi:10.1002/qj.3803.

Hill PG, Allan RP, Chiu JC, Stein TH (2016) A multisatellite climatology of clouds, radiation, and precipitation in southern West Africa and comparison to climate models. J Geophys Res: Atmospheres, 121(18), 10-857.

Hu ZZ, Huang B, Pegion K (2008) Low cloud errors over the southeastern Atlantic in the NCEP CFS and their association with lower-tropospheric stability and air-sea interaction. J Geophys Res: Atmospheres, 113(D12)

Hua W, Zhou L, Nicholson SE, Chen H, Qin M (2019) Assessing reanalysis data for understanding rainfall climatology and variability over Central Equatorial Africa. Clim Dyn, 53(1), 651-669. https://doi.org/10.1007/s00382-018-04604-0

Klein SA, Hartmann DL (1993) The Seasonal Cycle of Low Stratiform Clouds, J Climate, 6, 1587–1606.

Knippertz P, Fink AH, Schuster R, Trentmann J, Schrage JM, Yorke C (2011) Ultra-low clouds over the southern West African monsoon region. Geophys Res Lett, 38(21).

Koseki S, Imbol Koungue RA (2021) Regional atmospheric response to the Benguela Niñas. Int J Climatology, *41*, E1483-E1497. https://doi.org/10.1002/joc.6782

Lacaux JP, Delmas R, Kouadio G, Cros B, Andreae MO (1992) Precipitation chemistry in the Mayombe forest of equatorial Africa. J Geophys Res: Atmospheres, 97(D6), 6195-6206.

Lauer A, Hamilton K (2013) Simulating clouds with global climate models: A comparison of CMIP5 results with CMIP3 and satellite data. J Climate, 26(11), 3823-3845.

Lu Z, Liu X, Zhang Z, Zhao C, Meyer K, Rajapakshe C, ... & Penner JE (2018) Biomass smoke from southern Africa can significantly enhance the brightness of stratocumulus over the southeastern Atlantic Ocean. Proc Nat Acad Sci, 115(12), 2924-2929.

Mallet M, Solmon F, Nabat P, Elguindi N, Waquet F, Bouniol D, ... & Formenti P (2020) Direct and semi-direct radiative forcing of biomass-burning aerosols over the southeast Atlantic (SEA) and its sensitivity to absorbing properties: a regional climate modeling study. Atmospheric Chemistry and Physics, 20(21), 13191-13216. https://doi.org/10.5194/acp-20-13191-2020

Mallet M, Nabat P, Johnson B, Michou M, Haywood JM, Chen C, Dubovik O (2021) Climate models generally underrepresent the warming by Central Africa biomass-burning aerosols over the Southeast Atlantic. Sci Adv 7, 41, DOI: 10.1126/sciadv.abg9998

Merle J, Fieux M, Hisard P (1980) Annual signal and interannual anomalies of sea surface temperature in the eastern equatorial Atlantic Ocean. In Oceanography and Surface Layer Meteorology in the B/C Scale (pp. 77-101). Pergamon.

Meynadier R, de Coëtlogon G, Leduc-Leballeur M, Eymard L, Janicot S (2016) Seasonal influence of the sea surface temperature on the low atmospheric circulation and precipitation in the eastern equatorial Atlantic. Clim Dyn, 47(3), 1127-1142. DOI 10.1007/s00382-015-2892-7.

Myers TA, Scott RC, Zelinka MD et al. (2021) Observational constraints on low cloud feedback reduce uncertainty of climate sensitivity. Nat. Clim. Chang. **11,** 501–507. https://doi.org/10.1038/s41558-021-01039-0

Nam C, Bony S, Dufresne JL, Chepfer H (2012) The 'too few, too bright' tropical low-cloud problem in CMIP5 models. Geophys Res Lett, 39(21). https://doi.org/10.1029/2012GL053421

Neupane N (2016) The Congo basin zonal overturning circulation. Advances in Atmospheric Sciences, 33(6), 767–782. https://doi.org/10.1007/s00376-015-5190-8

Philippon N, Cornu G, Monteil L, Gond V, Moron V, Pergaud J, … Ngomanda A (2019) The light-deficient climates of western Central African evergreen forests. Envir Res Lett, 14(3), 1–11. https://doi.org/10.1088/1748-9326/aaf5d8

Philippon N, Ouhechou A, Camberlin P, Trentmann J, Fink AH, Maloba-Makanga JD, Morel B, Samba G (2021) Characterization of sunshine duration in Western Equatorial Africa : in-situ measurements vs SARAH-2 satellite estimates. Submitted to Journal of Applied Meteorology and Climatology.

Réjou-Méchain M, Mortier F, Bastin JF et al. (2021) Unveiling African rainforest composition and vulnerability to global change. Nature, 593, 90–94. https://doi.org/10.1038/s41586-021-03483-6

Richter I, Tokinaga H (2020) An overview of the performance of CMIP6 models in the tropical Atlantic: mean state, variability, and remote impacts. Clim Dyn **55,** 2579–2601. https://doi.org/10.1007/s00382-020-05409-w

Rienecker MM, Suarez MJ, Gelaro R, Todling R, Bacmeister J, Liu E, … Woollen J (2011) MERRA: NASA's Modern-Era Retrospective Analysis for Research and Applications. J Climate, 24(14), 3624–3648. https://doi.org/10.1175/JCLI-D-11-00015.1

Schrage JM, Fink AH (2012) Nocturnal Continental Low-Level Stratus over Tropical West Africa: Observations and Possible Mechanisms Controlling Its Onset. Mon Wea Rev, 140(6), 1794–1809. https://doi.org/10.1175/MWR-D-11-00172.1

Schuster R, Fink AH, Knippertz P (2013) Formation and Maintenance of Nocturnal Low-Level Stratus over the Southern West African Monsoon Region during AMMA 2006. J Atmospheric Sciences, 70(8), 2337–2355. https://doi.org/10.1175/JAS-D-12-0241.1

Servain J, Merle J (1993) Interannual Climate Variations Over the Tropical Atlantic Ocean. In: Shukla J. (eds) Prediction of Interannual Climate Variations. NATO ASI Series, vol 6. Springer, Berlin, Heidelberg. https://doi.org/10.1007/978-3-642-76960-3_8

Shannon LV, Boyd AJ, Bundrit GB, Taunton-Clark J (1986) On the existence of an El Niño–type phenomenon in the Benguela system, J. Mar. Sci., 44, 495–520.

Slingo JM (1987) The development and verification of a cloud prediction scheme for the ECMWF model. Quart. J. Roy. Meteor. Soc., 113, 899–927.

Smith A, Lott N, Vose, R (2011) The integrated surface database: Recent developments and partnerships. Bull American Met Soc, 92(6), 704–708. https://doi.org/10.1175/2011BAMS3015.1

Sun F, Hall A, Qu X (2011) On the relationship between low cloud variability and lower tropospheric stability in the Southeast Pacific. Atmospheric Chemistry and Physics, 11(17), 9053-9065.

Trewartha GT (1981) The Earth's Problem Climates, University of Wisconsin Press, 371 pp

Trzaska S, Robertson AW, Farrara JD, Mechoso CR (2007) South Atlantic variability arising from air–sea coupling: local mechanisms and tropical–subtropical interactions. J Climate, 20, 3345–3365, doi:10.1175/JCLI4114.1.

Tschirhart G (1959) Les perturbations atmosphériques intéressant l'AEF méridionale. Monogr. Mét. Nat., Paris, 13, 32 p.

Vaughan MA, Powell KA, Winker DM, Hostetler CA, Kuehn RE, Hunt WH, … McGill MJ (2009) Fully Automated Detection of Cloud and Aerosol Layers in the CALIPSO Lidar Measurements. J Atmospheric and Oceanic Technology, 26(10), 2034–2050. https://doi.org/10.1175/2009JTECHA1228.1

Voldoire A, Saint-Martin D, Sénési S, Decharme B, Alias A, Chevallier M, et al. (2019) Evaluation of CMIP6DECK experiments with CNRM-CM6-1. J Advances in Modeling Earth Systems,11, 2177–2213. https://doi.org/10.1029/2019MS001683

Webb MJ, Andrews T, Bodas-Salcedo A, Bony S, Bretherton CS, Chadwick R, … Watanabe M (2017) The Cloud Feedback Model Intercomparison Project (CFMIP) contribution to CMIP6. Geosci. Model Dev, 10, 359–384. https://doi.org/10.5194/gmd-10-359-2017

Wood R (2012) Stratocumulus clouds. Mon Wea Rev, Vol. 140, pp. 2373–2423. https://doi.org/10.1175/MWR-D-11-00121.1

Xu Z, Chang P, Richter I, Tang G (2014) Diagnosing southeast tropical Atlantic SST and ocean circulation biases in the CMIP5 ensemble. Clim Dyn, 43(11), 3123-3145.

Zelinka MD, Randall DA, Webb MJ, Klein SA (2017) Clearing clouds of uncertainty. Nature Climate Change 7, 674–678, https://doi.org/10.1038/nclimate3402

Zhang C (1993) Large-Scale Variability of Atmospheric Deep Convection in Relation to Sea Surface Temperature in the Tropics. J Climate, *6*(10), 1898-1913.

List of tables

856 Table 1: Datasets used in the study together with the corresponding low cloud definition.

857

Data base/ Model	Spatial scale (atmosphere)	Retained period	Type of data	# ensemble members (coupled/ atmosphere-only)	Definition of low clouds
CALIOP	200km	2006–2019	Satellite (lidar)	-	LC fraction (levels >680hPa)
ISD	Synoptic stations	1979–2014	Weather observations	-	LC frequency (<2000 m)
EECRA	Synoptic Stations	1979–2009	Edited weather observations	-	LC fraction (<2000 m)
ERA5	30km	1979–2014	Reanalysis	-	LC fraction (levels >0.8 surface pressure)
MERRA2	50km	1980–2014	Reanalysis	-	LC fraction (levels >700hPa)
CNRM	250km	1979–2014	Simulations	3/1	LC fraction (levels >680hPa)
IPSL	250km	1979–2014	Simulations	3/1	
E3SM	100km	1979–2014	Simulations	3/3	
MIROC	250km	1979–2014	Simulations	1/1	
MOHC	250km	1979–2014	Simulations	1/1	
MRI	100km	1979–2014	Simulations	1/1	
GFDL	100km	1979–2014	Simulations	1/1	
NCAR	100km	1979–2014	Simulations	1/1	

858

859

Table 2: Correlations between interannual variations (1979–2014) of JJAS low cloud cover in ERA5, ISD and EECRA. All correlations are significant at P<0.01.

	NW-GABON		**NE-GABON**	
	R	Number of years	R	Number of years
ISD vs. EECRA	0.95	17	0.93	11
ERA5 vs. ISD	0.78	26	0.84	10
ERA5 vs. EECRA	0.77	19	0.82	18

867 List of figures

868

mean of a given year. Regression lines are shown when the cloud fraction significantly correlates ($p<0.05$) with SST.

Figure 12: Same as figure 10 but for CMIP6 atmosphere-only simulations

Figure 13: As in figure 11 but for LC fraction in NW-Gabon versus Lower-Tropospheric Stability (LTS) between 925 and 700 hPa over Gabon (10-12°E, 3°S-1°N).

Figure 14: Correlations between interannual variations (1979–2014) of ERA5 JJAS LC fraction in NW-Gabon and different atmospheric fields. Top panels: correlation maps for ERA5 (thick white lines: 0.05 significance level; thin white lines: -0.6 and 0.6 isocorrelations). Central panels: total correlations between MW-Gabon LC fraction and regional indices computed over the yellow boxes shown on the maps (stars indicate correlations significant at $p<0.05$, and big stars at $p<0.01$), for ERA5 and CMIP6 coupled simulations. Bottom panels: same as central panels but for partial correlations independently of SST variations southwest of Gabon.

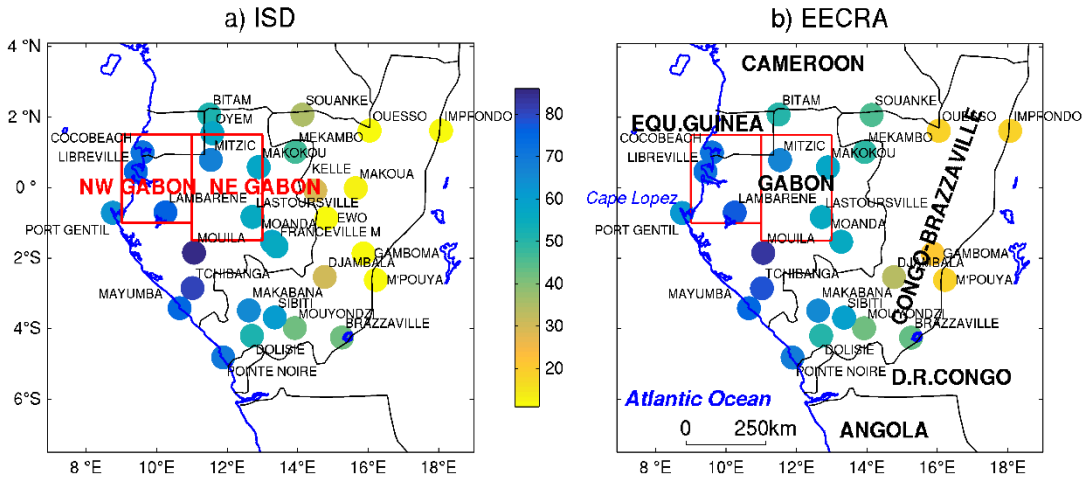

Figure 1: Map of Western Equatorial Africa with the surface stations extracted from the ISD (a) and EECRA (b) databases to compute low cloud statistics. Colour dots: mean JJAS low cloud frequency (a) and low cloud fraction (b), in percentages. Red boxes border the areas for the LCC regional indices.

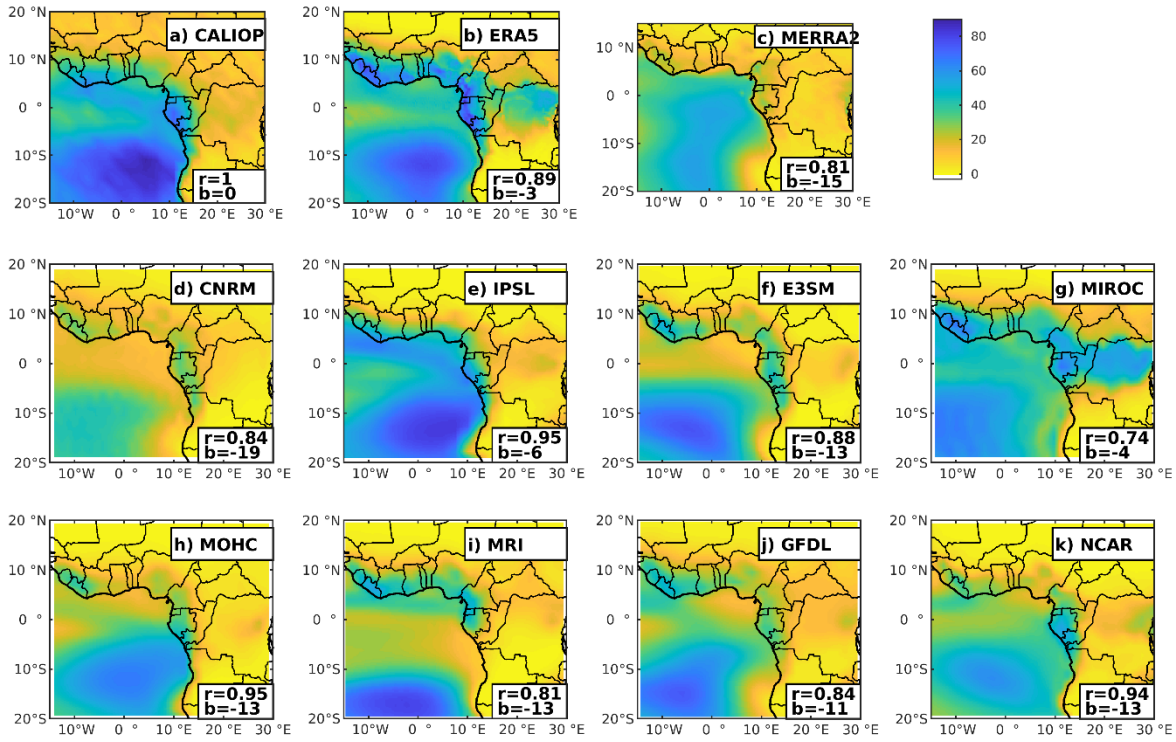

Figure 2: JJAS mean low cloud fraction (in %) for CALIOP (a), ERA5 (b), MERRA2 (c) and CMIP6 coupled simulations: CNRM (d), IPSL (e), E3SM (f), MIROC (g), MOHC (h), MRI (i), GFDL (j), NCAR (k). Means are computed over the period 1979–2014 (1980–2014 for MERRA2). In the boxes, r is the pattern correlation with CALIOP and b is the mean bias (in % cloud fraction).

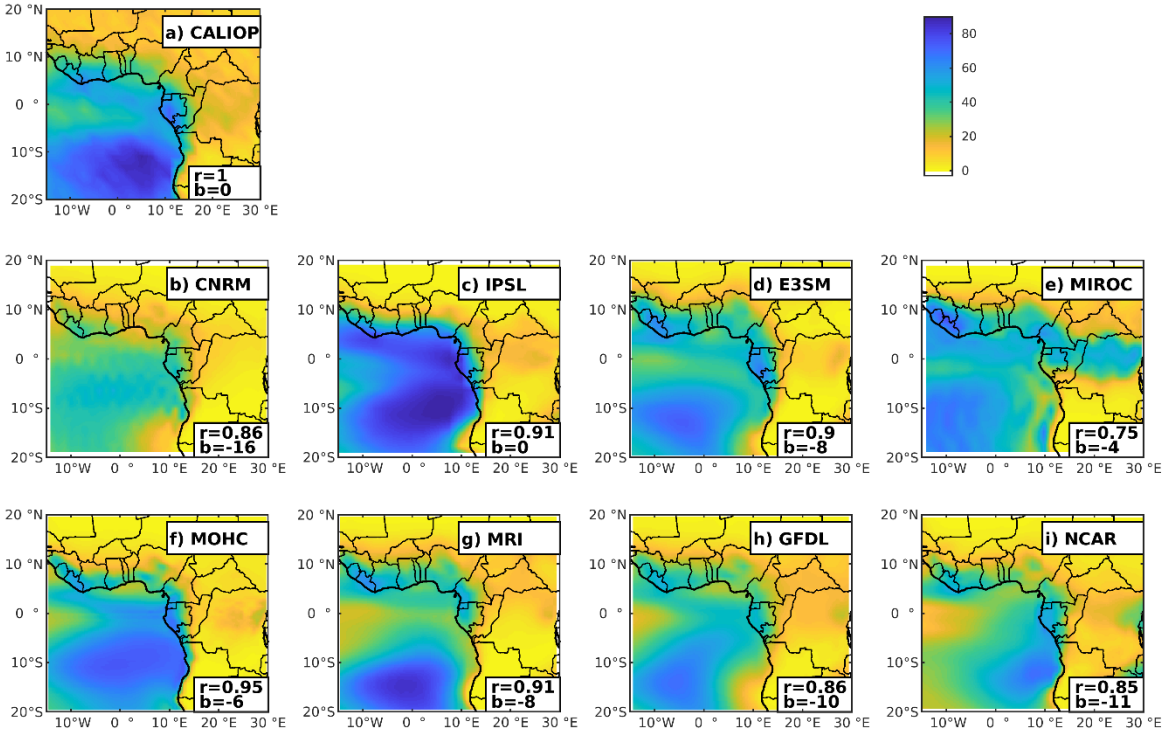

Figure 3: Same as figure 2 but for CALIOP (a) and CMIP6 atmosphere-only simulations from CNRM (b), IPSL (c), E3SM (d), MIROC (e), MOHC (f), MRI (g), GFDL (h), NCAR (i).

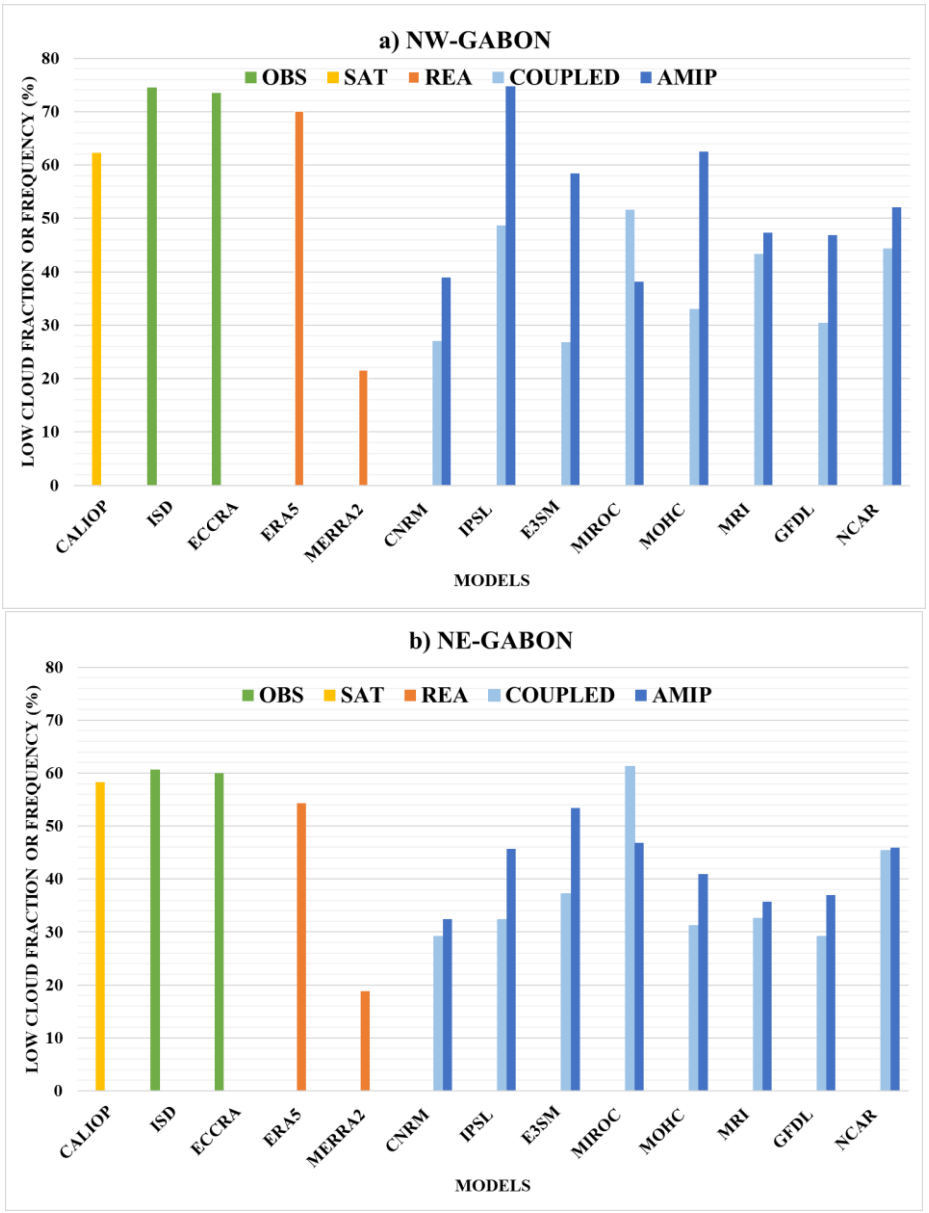

Figure 4: JJAS mean low cloud cover over NW Gabon (a) and NE Gabon (b). See table 1 for the definition of low cloud cover and the period used for computation in each dataset.

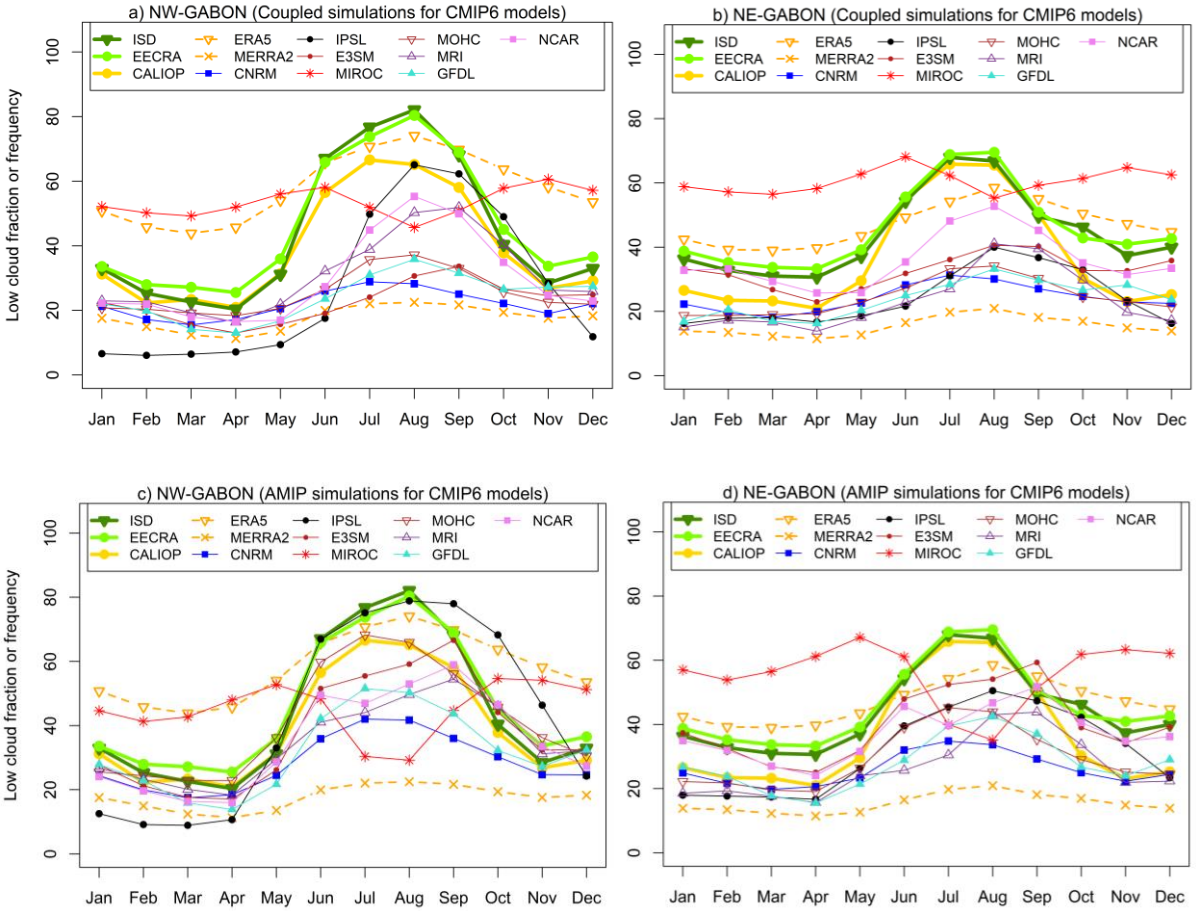

Figure 5: Mean annual cycle of low cloud cover over NW Gabon (a, c) and NE Gabon (b, d). CMIP6 coupled simulations are displayed in (a) and (b), and atmosphere-only simulations in (c) and (d).

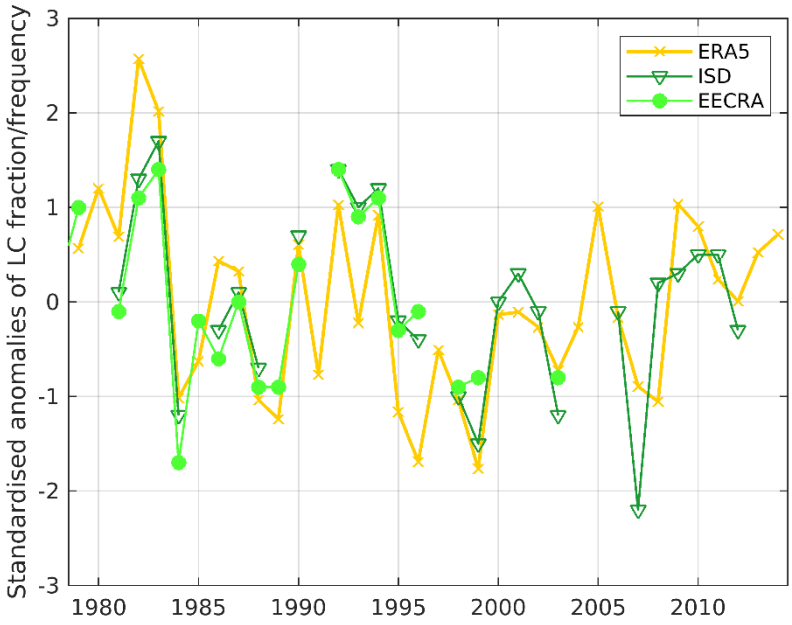

940

941 Figure 6: Interannual variations of JJAS low cloud cover between 1979 and 2014 in NW Gabon in
942 ERA5 reanalysis (LC fraction) as well as in ISD (LC frequency) and EECRA (LC fraction) observations.

943

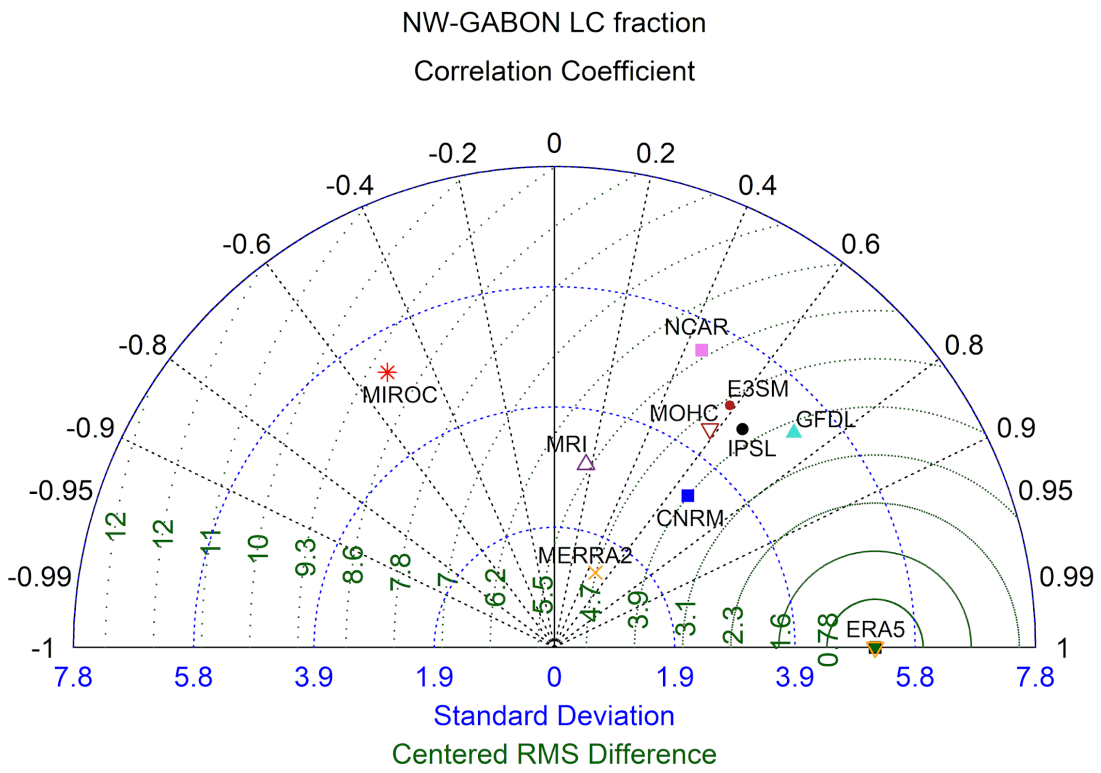

Figure 7: Taylor diagram of JJAS 1979–2014 NW-Gabon low cloud fraction in MERRA2 and CMIP6 atmosphere-only simulations, with ERA5 as the reference. Black dotted lines: correlation coefficients. Blue dotted lines: standard-deviations. Green lines: RMSE.

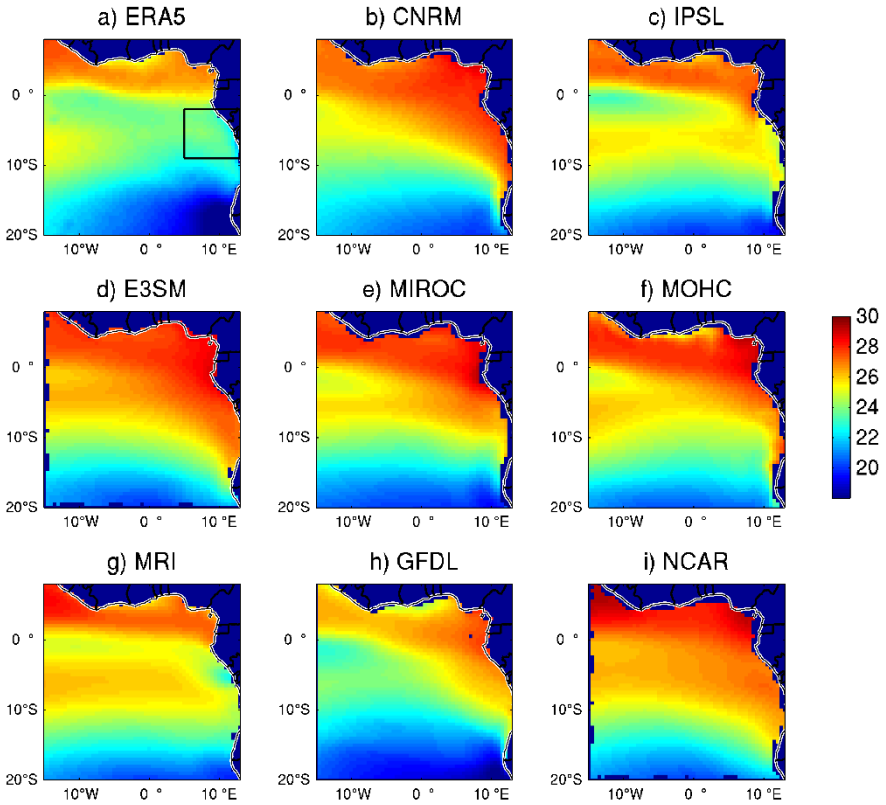

Figure 8 : JJAS mean SST (1979–2014, °C) over the South Atlantic Ocean in ERA5 (a) and CMIP6 coupled simulations: CNRM (b), IPSL (c), E3SM (d), MIROC (e), MOHC (f), MRI (g), GFDL (h), NCAR (i). The location of the Gabon SST index is shown on panel (a).

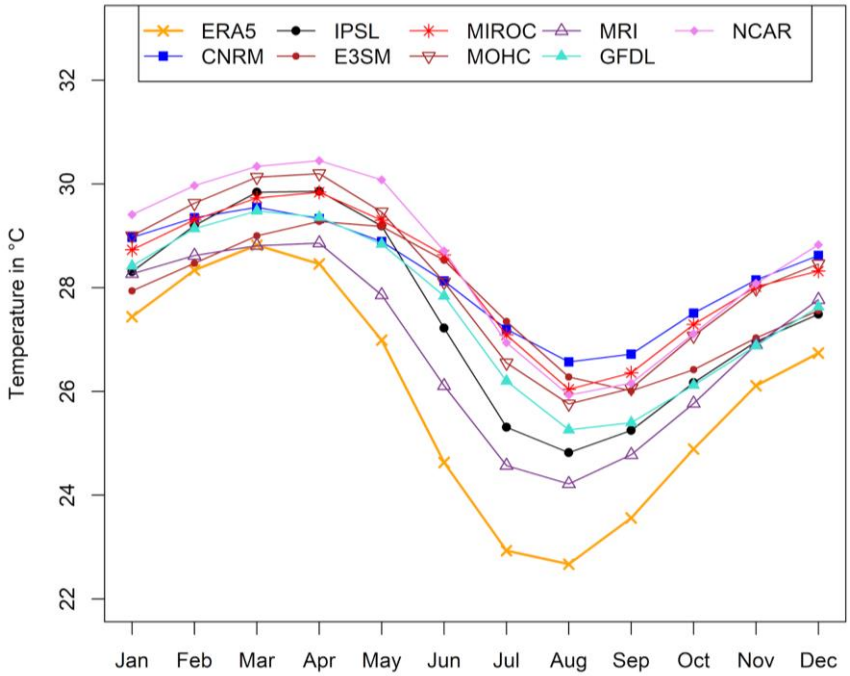

Figure 9 : Mean annual cycle (1979–2014) of SST over the region [9–2°S, 5–13°E] in the Atlantic Ocean southwest of Gabon (boxed area on figure 8a): ERA5 reanalysis and CMIP6 coupled simulations.

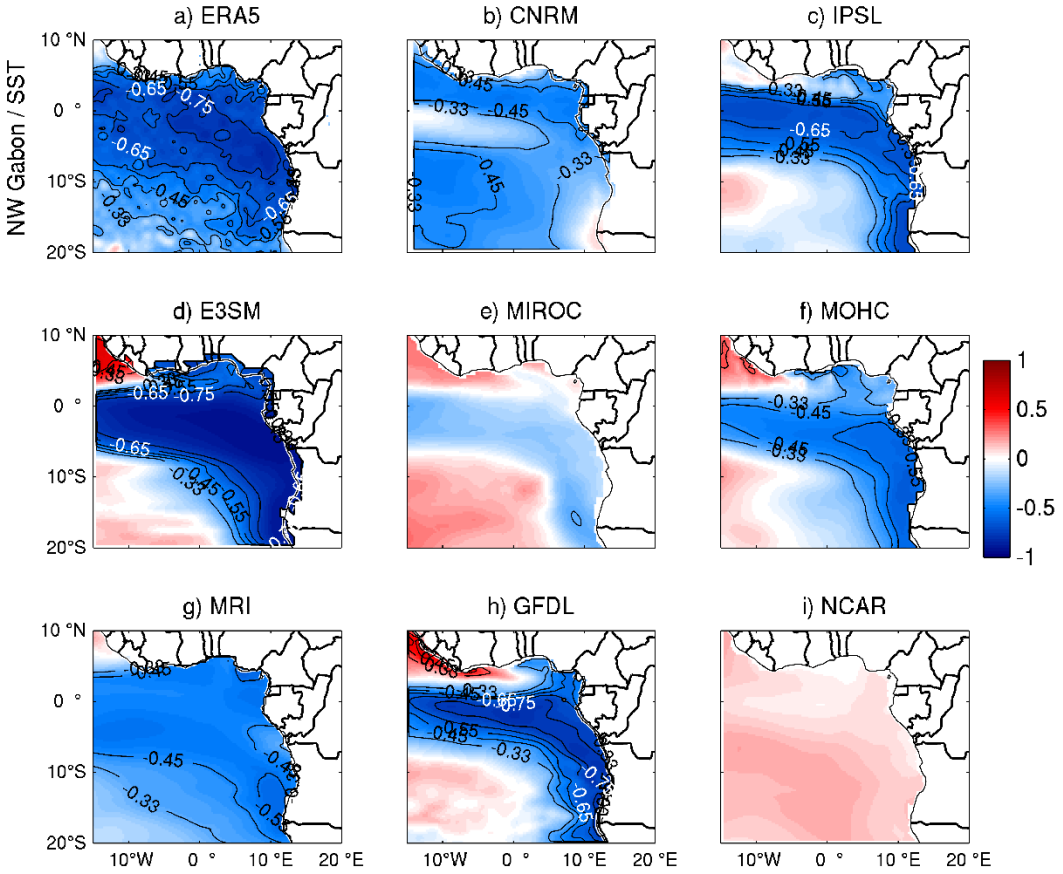

Figure 10: Internal correlations between interannual variations (1979-2014) of JJAS SST and low cloud cover in NW-Gabon, in ERA5 and in each CMIP6 coupled model. Values above 0.33 / below -0.33 are significant at P<0.05.

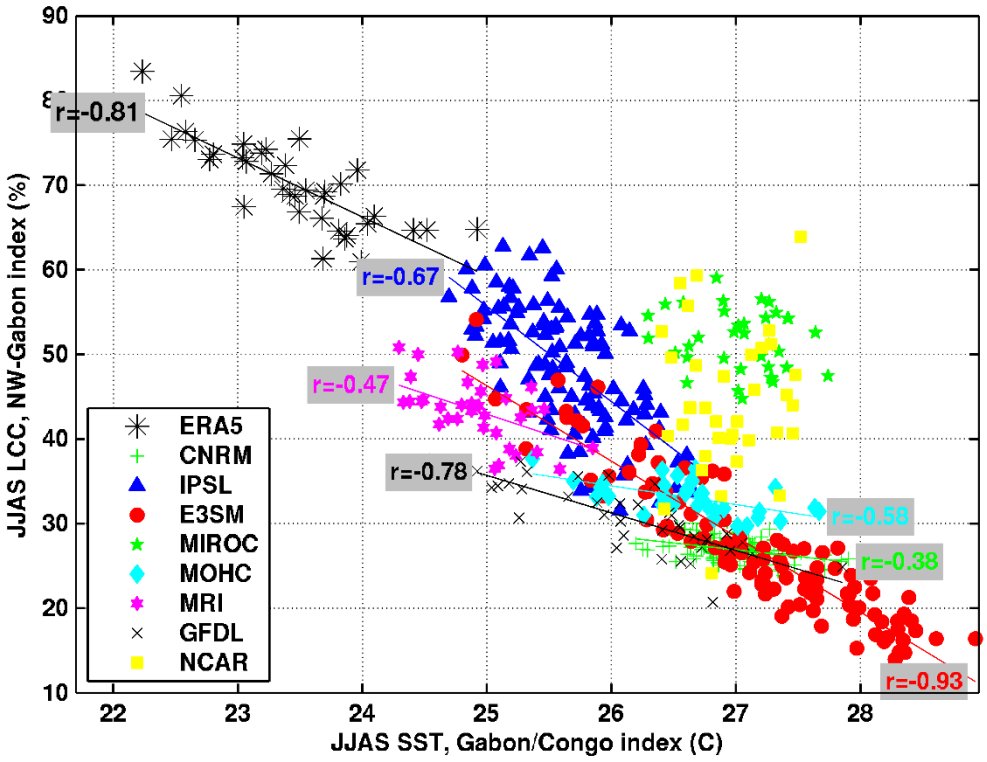

966

967 Figure 11: Scatter plot of LC fraction in NW-Gabon versus SST over the Atlantic Ocean southwest of
968 Gabon [9–2°S, 5–13°E], for ERA5 and for each of the 8 CMIP6 coupled models. Each marker is the
969 JJAS mean of a given year. Regression lines are shown when the cloud fraction significantly correlates
970 ($p<0.05$) with SST.

971

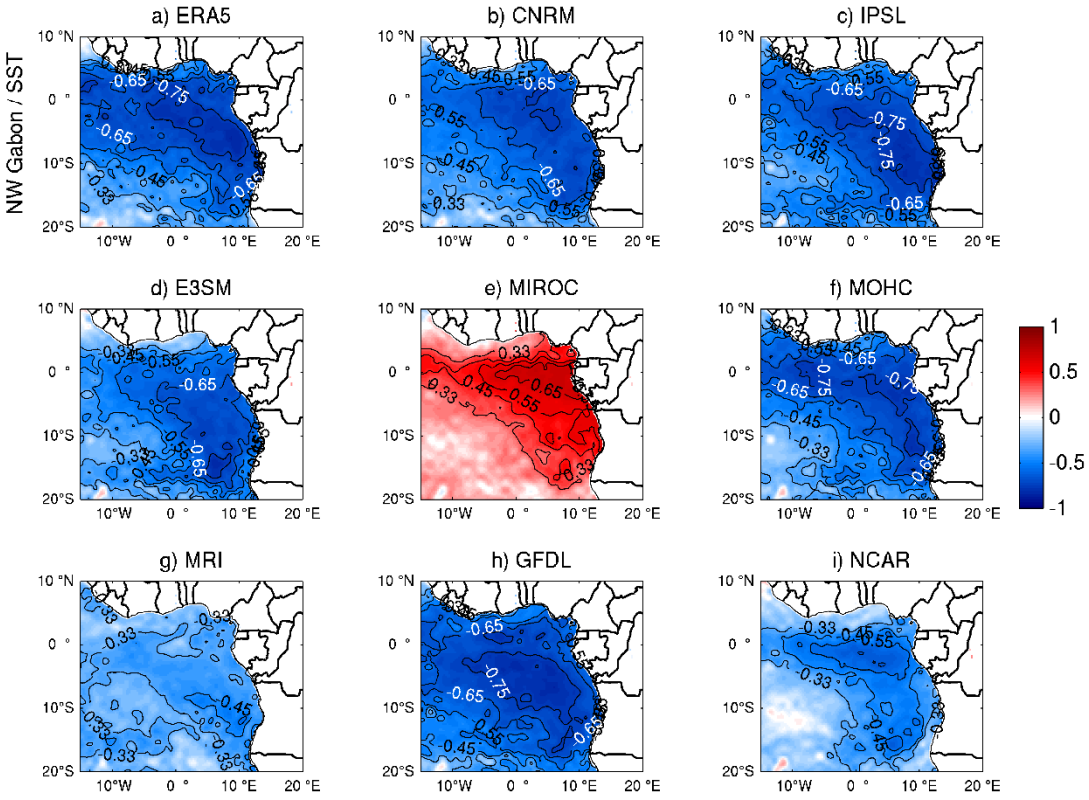

Figure 12 : Same as figure 10 but for CMIP6 atmosphere-only simulations

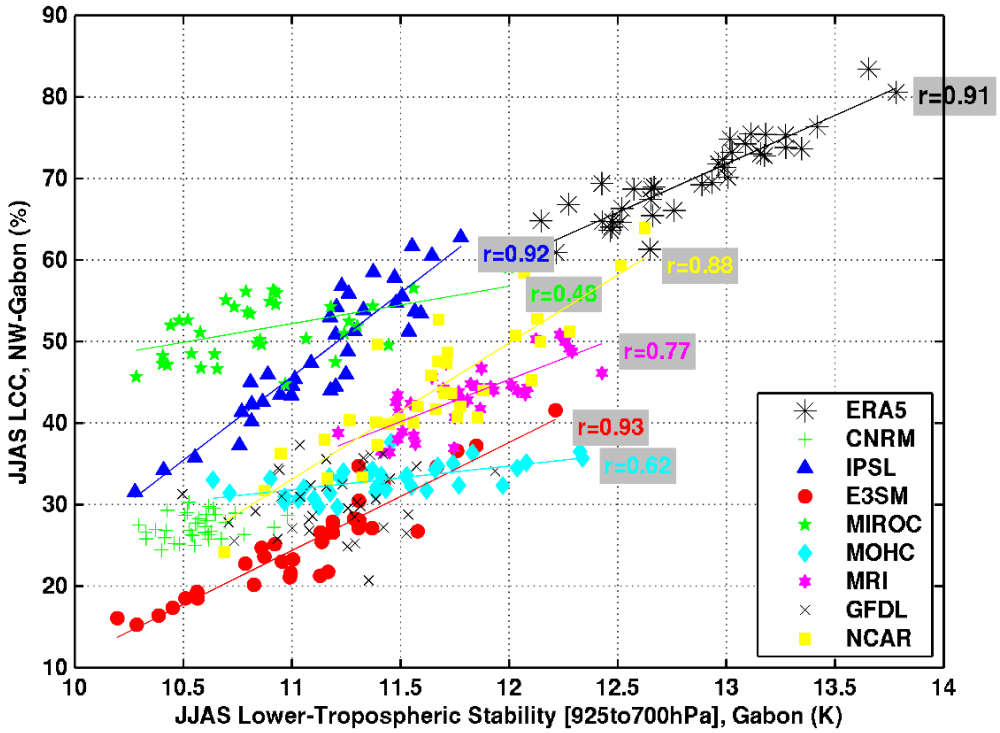

Figure 13: As in figure 11 but for LC fraction in NW-Gabon versus Lower-Tropospheric Stability (LTS) between 925 and 700 hPa over Gabon (10-12°E, 3°S-1°N).

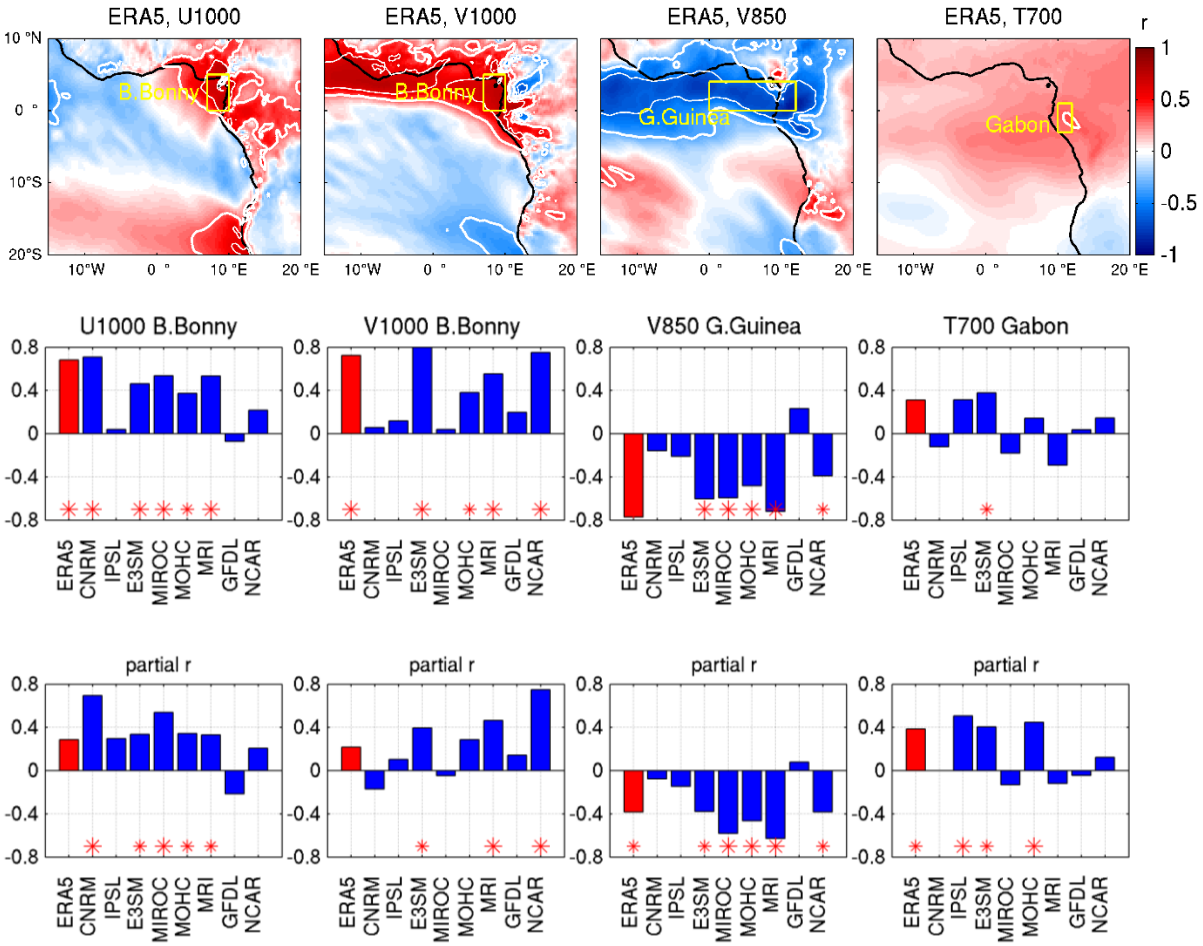

Figure 14: Correlations between interannual variations (1979–2014) of ERA5 JJAS LC fraction in NW-Gabon and different atmospheric fields. Top panels: correlation maps for ERA5 (thick white lines: 0.05 significance level; thin white lines: -0.6 and 0.6 isocorrelations). Central panels: total correlations between MW-Gabon LC fraction and regional indices computed over the yellow boxes shown on the maps (stars indicate correlations significant at p<0.05, and big stars at p<0.01), for ERA5 and CMIP6 coupled simulations. Bottom panels: same as central panels but for partial correlations independently of SST variations southwest of Gabon.